AD-A031 500 HARVARD COLL OBSERVATORY CAMBRIDGE MASS F/G 3/2
INVESTIGATIONS OF SOLAR FLARES, QUIET AND ACTIVE REGIONS BASED --ETC(U)
SEP 76 G L WITHBROE, J E VERNAZZA F19628-74-C-0018
UNCLASSIFIED AFGL-TR-76-0217 NL

1 OF 1
ADA031500

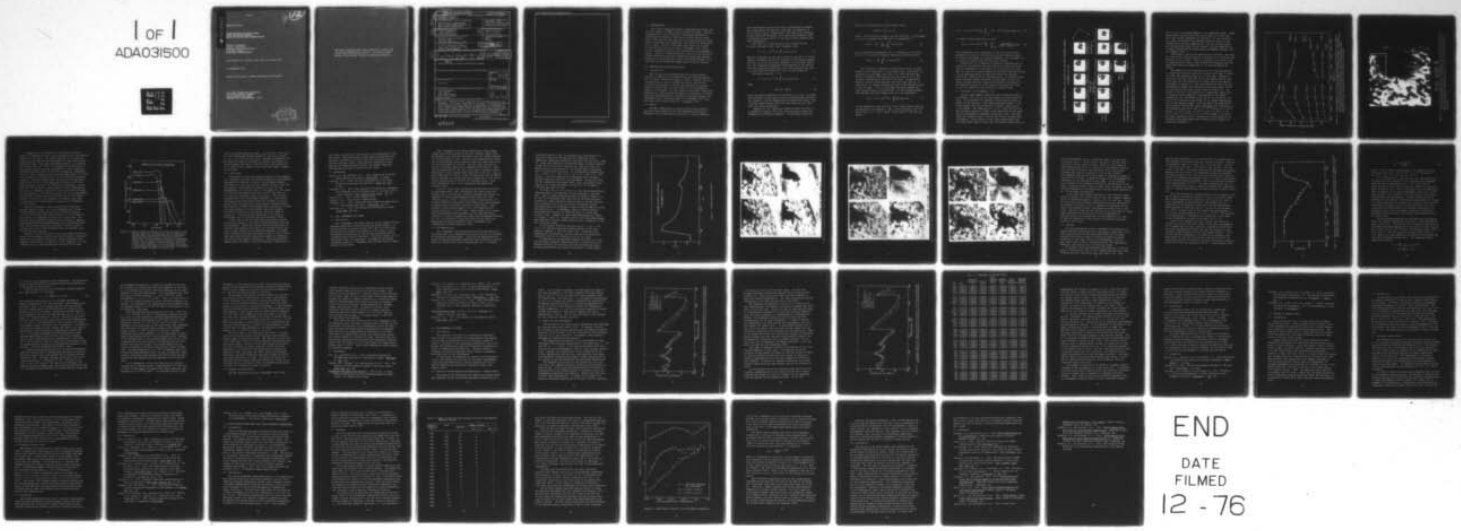

END
DATE FILMED
12 - 76

12

AFGL-TR-76-0217

INVESTIGATIONS OF SOLAR FLARES, QUIET AND ACTIVE REGIONS BASED ON EUV AND RADIO OBSERVATIONS

George L. Withbroe
Jorge E. Vernazza
Harvard College Observatory
60 Garden Street
Cambridge, Massachusetts

Final Report for Period 1 July 1973 to 30 June 1976

30 September 1976

Approved for public release; distribution unlimited

AIR FORCE GEOPHYSICS LABORATORY
AIR FORCE SYSTEMS COMMAND
UNITED STATES AIR FORCE
HANSCOM AFB, MASSACHUSETTS 01731

Unclassified

SECURITY CLASSIFICATION OF THIS PAGE (When Data Entered)

REPORT DOCUMENTATION PAGE

READ INSTRUCTIONS BEFORE COMPLETING FORM

1. REPORT NUMBER: AFGL-TR-76-0217	2. GOVT ACCESSION NO.
3. RECIPIENT'S CATALOG NUMBER	
4. TITLE (and Subtitle): INVESTIGATIONS OF SOLAR FLARES, QUIET AND ACTIVE REGIONS BASED ON EUV AND RADIO OBSERVATIONS	5. TYPE OF REPORT & PERIOD COVERED: Scientific. Final. 1 July 1973 to 30 June 1976
	6. PERFORMING ORG. REPORT NUMBER
7. AUTHOR(s): George L. Withbroe, Jorge E. Vernazza	8. CONTRACT OR GRANT NUMBER(s): F19628-74-C-0018
9. PERFORMING ORGANIZATION NAME AND ADDRESS: Harvard College Observatory, 60 Garden Street, Cambridge, Massachusetts 02138	10. PROGRAM ELEMENT, PROJECT, TASK AREA & WORK UNIT NUMBERS: 62101F, 46430302
11. CONTROLLING OFFICE NAME AND ADDRESS: Air Force Geophysics Laboratory, Hanscom AFB, Massachusetts 01731, Monitor/ Ron Straka/PHP	12. REPORT DATE: 30 September 1976
	13. NUMBER OF PAGES: 48
14. MONITORING AGENCY NAME & ADDRESS (if different from Controlling Office)	15. SECURITY CLASS. (of this report): Unclassified
	15a. DECLASSIFICATION/DOWNGRADING SCHEDULE

Final Rept. 1 Jul 73 - 30 Jun 76

12 50 p.

16. DISTRIBUTION STATEMENT (of this Report)

Approved for public release; distribution unlimited.

17. DISTRIBUTION STATEMENT (of the abstract entered in Block 20, if different from Report)

ACCESSION for	
NTIS	White Section ☒
DDC	Buff Section ☐
UNANNOUNCED	☐
JUSTIFICATION	
BY	
DISTRIBUTION/AVAILABILITY CODES	
Dist.	AVAIL. and/or SPECIAL
A	

18. SUPPLEMENTARY NOTES

Tech Other

19. KEY WORDS (Continue on reverse side if necessary and identify by block number)

Solar Chromosphere
Solar Flares
Solar Radio Emission
Solar Active Regions
Coronal Holes

20. ABSTRACT (Continue on reverse side if necessary and identify by block number)

This report summarizes several investigations of the quiet and active solar atmosphere. It includes a discussion of a technique for studying the physical conditions in active region loops and the application of the technique to loops in McMath region 12628 and loops associated with the 7 September 1973 proton flare in McMath region 12507. The report also summarizes some work on coronal hole models, models for the chromosphere and an investigation of relationships between flare rates and 8.6 mm brightness temperatures.

DD FORM 1 JAN 73 1473 EDITION OF 1 NOV 65 IS OBSOLETE

Unclassified

SECURITY CLASSIFICATION OF THIS PAGE (When Data Entered)

163450

1.0 INTRODUCTION

This report summarizes several investigations carried out with the support of AFCRL contract F19628-74-C-0018. Section 2 discusses some of the theoretical techniques developed to investigate the physical conditions in active region loops. These techniques are then applied to the analyses of an active region loop system that undergoes a disruption not associated with a flare. Section 3 describes some results of a study of the importance 2B proton flare 7 September, 1973, while Section 4 summarizes work on the construction of chromospheric models. Section 5 discusses briefly results of two studies of coronal holes while Section 6 summarizes previously reported results of an investigation on the relationship between flare rates and 8.6 mm brightness temperatures of active regions.

2.0 ANALYSIS OF ACTIVE REGION LOOPS

2.1 Introduction

Much of the activity associated with active regions consists of changes in the temperatures and densities and/or flow of plasma confined by magnetic fields. Because the field configurations in active regions are closed, many of the features and phenomena in active regions appear as coronal loops or arches whose feet are rooted in the chromospheric layers of the regions. In this report we describe a new method developed for investigating the physical conditions in coronal loops and its application to studies of two loop systems, one associated with a non-flare event on 24 November, 1973, and the other with a proton flare on 7 September, 1973.

2.2 Theory

The best observations of active region loops currently available were obtained by the ATM experiments on Skylab. Because of their high spatial resolution, a few arc seconds,

these experiments provide data that is particularly valuable for investigating the physical conditions and dynamics of active region loops. Consequently, the theoretical framework we have developed (Withbroe, 1975; Levine and Withbroe, 1976) is designed for application to the type of data acquired from these experiments.

The flux F on an XUV emission line is given by the relation (Pottasch, 1964, 1967; Withbroe, 1970)

$$F = 2.2 \times 10^{-15} \, Af \int g \, G(T) \, n_e^2 \, dV, \tag{1}$$

where F is measured at the sun in units of erg sec^{-1}, A is the chemical abundance relative to hydrogen of the element forming the line, f is the oscillator strength, g is the Gaunt factor, G(T) is a temperature-dependent term depending on the excitation and ionization properties of the atom producing the line; n_e is the electron density cm^{-3} and V is the volume cm^3.

We rewrite equation (1) as

$$F = 2.2 \times 10^{-15} \, Af \int g \, G(T) \, Q(T) \, dT, \tag{2}$$

where

$$Q(T) \, dT = n_e^2 \, dV \tag{3}$$

gives the emission measure in the range T to T + dT. An iterative procedure is then used to find a self-consistent function Q(T) based on a set of observations in several EUV lines. The iteration method assures that the final function Q(T) reproduces the input intensities.

Knowing Q(T) at a particular position along the loop, it is possible to predict the local loop structure, within the framework of cylindrical geometry. If the length along the

loop is L the cylindrical volume element gives

$$Q(T)dT = n_e^2\, 2\pi L\, r\, dr \tag{4}$$

where r is the radial distance from the loop axis. If we assume $P = n_e T$ is constant then equation (4) integrates to

$$r^2(T) - r_o^2 = \frac{1}{\pi L P^2} \int_{T_o}^{T} T^2\, Q(T)\, dT, \tag{5}$$

with T_o being the temperature at r_o. Allowing r_o to be zero for $T_o = 0$, we have an analytic expression for the quantity

$$r(T)P = \left(\frac{1}{\pi L} \int_{o}^{T} T^2\, Q(T)dT \right)^{1/2} . \tag{6}$$

The intensity I emitted by a particular line of a given element in the range T to T + dT varies as $dI \sim Q(T)\, gG(T)\, dT$, allowing us to plot $\frac{dI}{dT} \sim Q(T)\, gG(T)$ vs. r(T)P and find the amount of emission from each line at any value of rP in the cylinder representing a section of the loop. As observers, however, we see a total emission from the loop, that is, at each point, an integral through the loop of the emission along a line of sight. If S is a straight line path through the loop, perpendicular to the axis and ρ is the distance between the loop axis and the closest point of S the expression,

$$I(\rho) = 1.75 \times 10^{-16}\, Af \int_S n_e^2\, gG(T)\, dS, \tag{7}$$

is the emission in ergs cm^{-2} sec^{-1} str^{-1} that would be seen by an observer at one end of S. Then, noting that $dr = \cos\theta\, dS$ where $\cos^2\theta = 1 - \rho^2/r^2$, $n_e^2\, dS = (2\pi rL \cos\theta)^{-1}\, Q(T)\, dT$, we obtain

$$I(\rho) = 5.57 \times 10^{-17} \, Af \, \frac{1}{L} \int_{T(\rho)}^{\infty} (r^2 - \rho^2)^{-1/2} \, Q(T) \, gG(T) \, dT. \quad (8)$$

In terms of known quantities, we find

$$I(\rho P) = 5.57 \times 10^{-17} \, \frac{AfP}{L} \int_{T(\rho P)}^{\infty} \frac{Q(T) gG(T)}{(r^2 P^2 - \rho^2 P^2)^{1/2}} \, dT. \quad (9)$$

This expression can be evaluated for any line whose atomic parameters are given, once the function Q(T) has been found. It tells us the amount of emission observed, and its shape, as a function of radius from the loop axis times P.

Notice that it is possible to obtain a consistent set of values for the function Q(T) from data of a given resolution that is averaged over a section of a loop and then use that Q(T) to find I(ρP), which predicts the emission from any single line at positions which include sizes below the original resolution. Because of the unknown factor P no absolute information has been gained this way, but the shape of the I(ρP) curve, coupled with size restrictions based on the extent of the observed emissions, allow limits to be placed on P and on the true extent of loop emission in various lines.

2.3 The Event of 24 November, 1973

Active region McMath 12628 was first observed by ATM on 23 November, 1973, one or two days after it rotated onto the disk. On 24 November the sequence of observations shown in Figure 2-1was obtained. Each spectroheliogram shows a 5 arc minute square area of the sun with a spatial resolution of 5 arc seconds. The observations in O VI λ 1032 from 0152 to 0214 UT show a series of loops in the upper half of the image that are increasing in emission during this time. The same loops are visible in Mg X λ 625 at 0214 UT as a broader arch of emission. Lines formed at even lower temperatures than O VI show these loops as thin tubes of emission whose width is

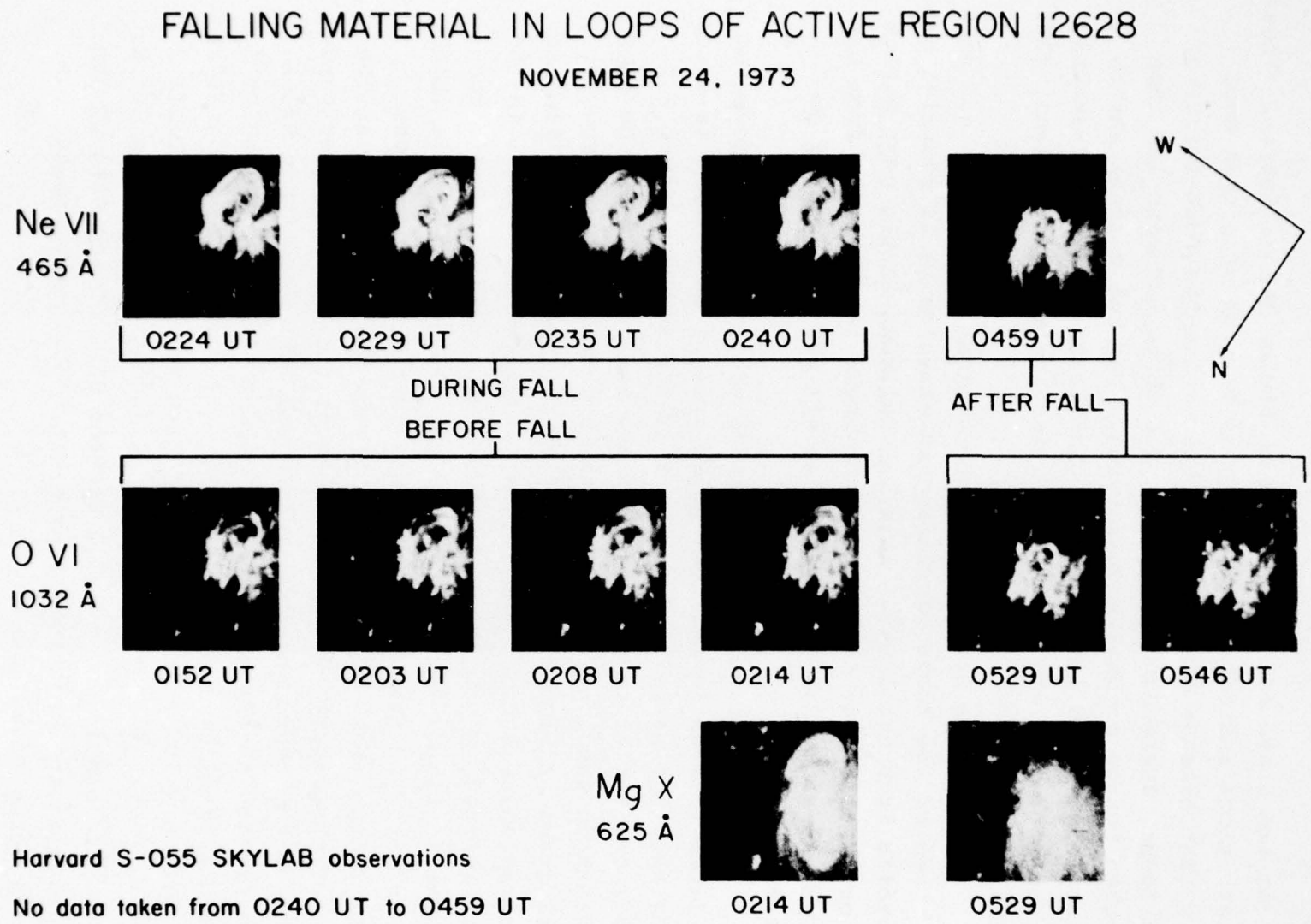

Figure 2-1. Spectroheliograms obtained by the Harvard ATM experiment, showing the dramatic draining of material from a collection of active region loops.

one or two 5 arc second elements of the spectroheliogram. These observations indicate that the loops consist of a thin cool core that extends downwards all the way to the foot points of the loops, surrounded by an extended sheath of material that reaches hotter coronal temperatures. The hot coronal sheath surrounding these loops is also visible in X-ray observations of these regions made by other Skylab instruments (Vaiana, 1976 and Vorpahl, 1976).

From 0224 to 0240 UT the observations in Ne VII λ 465 show the tops of the loops decreasing in emission as if material were draining from the loops. This is confirmed in the next series of observations at 0459 to 0546 UT where the emission from the loops has virtually disappeared at all EUV wavelengths observed.

The behavior of the intensities of the loops as measured in lines from different ions gives insight as to what is occurring when the material drains out of the loops. Figure 2-2 gives the variation with time of the EUV fluxes from the area containing the loop complex in the upper half of the spectroheliograms in Figure 2-1. The flux plotted for each line was determined by summing the intensities from each pictal in the area defined by the large outline drawn in Figure 2-3. The fluxes in Figure 2-2 are plotted on a logarithmic scale which is adjusted so that spectral lines formed at the highest temperature, Mg X 625 Å and Si XII 521 Å, are plotted at the top of the figure and lines formed at the lowest temperatures, such as the hydrogen Lyman α line and Lyman continuum 822 Å, are plotted at the bottom. Mean temperatures of formation for the different ions are Si XII, 2.5×10^6 K; Mg X, 1.4×10^6 K; Ne VII, 6×10^5 K; O VI, 3×10^5 K; O IV, 2×10^5 K; O III, 10^5 K; C III, 9×10^4 K; C II, 5×10^4 K; Lyman α, 2×10^4 K; and Lyman continuum, 10^4 K. Between 0214 UT and 0224 UT the grating in the spectrometer was rotated so as to change the lines being measured.

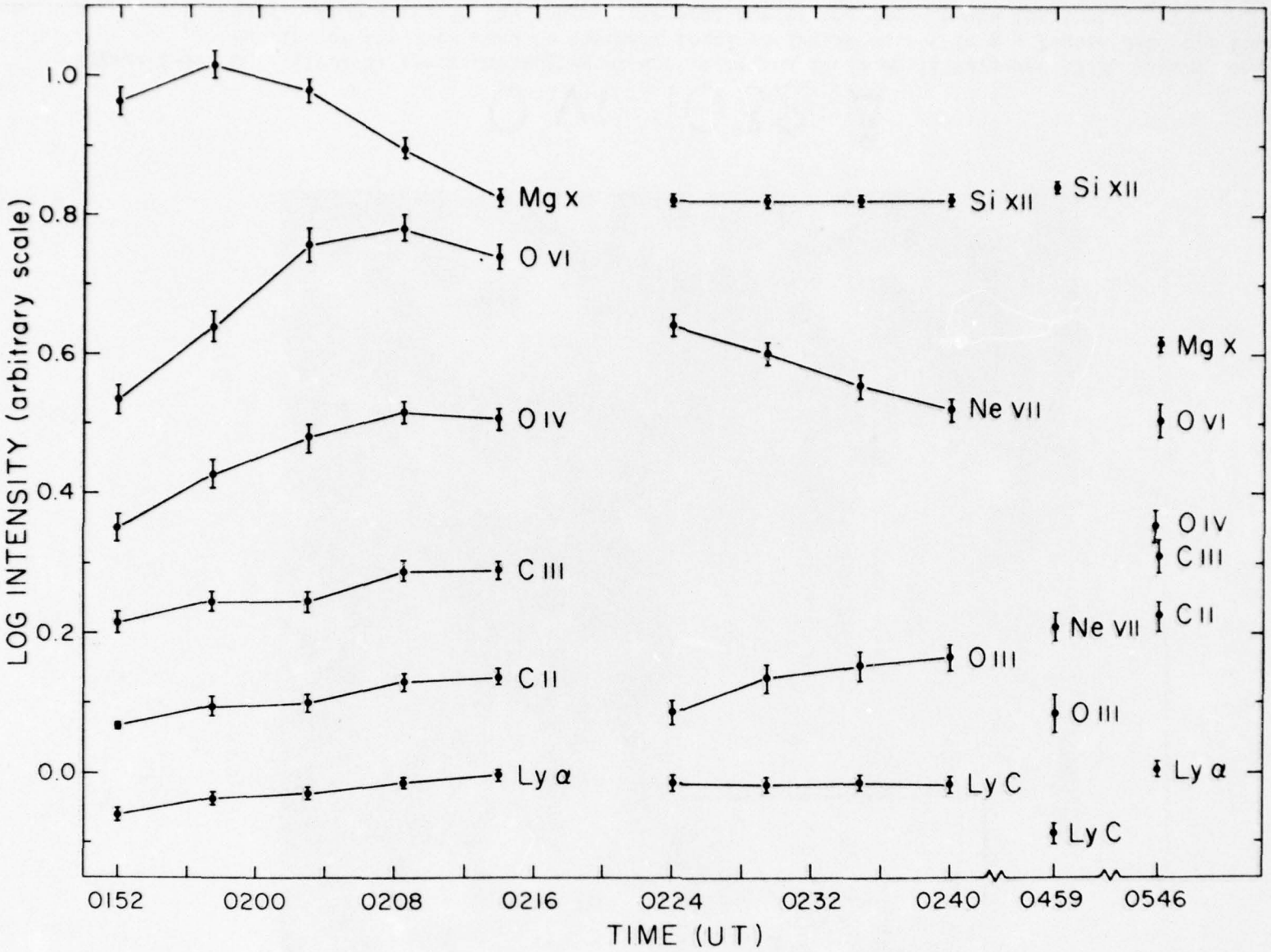

Figure 2-2. Energy radiated by the portion of the loop system outlined in Figure 2-3 as a function of time. Different sets of emission lines cover different intervals of time because the spectrometer grating position was changed. Lines formed at higher temperatures have been placed nearer the top of the graph to make physical interpretation easier. Comparison of absolute intensities is thus not possible from this graph.

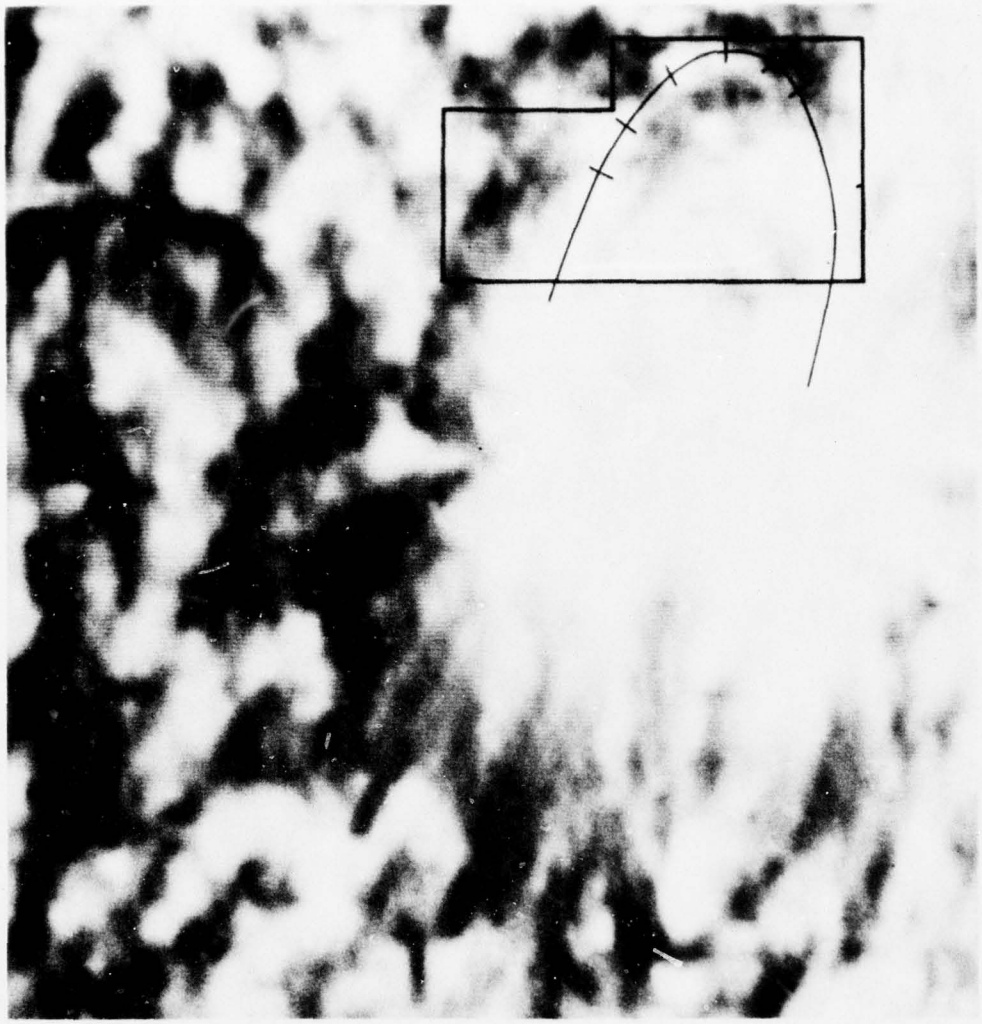

Figure 2-3. O VI (1032 Å) spectroheliogram of active region 12628 on 24 November 1973, showing the outline of the area used to estimate total radiative output (e.g., Figure 2-2) and total mass. Also shown is the approximate position of the loop chosen for further study (cf. Levine and Withbroe 1976) and the positions along this loop at which models were constructed.

A comparison of the behavior of the fluxes plotted in Figure 2-2 suggests the most likely explanation for the observed behavior of the loops. Hot coronal material in the loops is cooling and falling into the chromosphere at both ends of each individual loop. Under this hypothesis material at a temperature hotter than 1.4×10^6 K, the temperature at which Mg X is the dominant ionization stage of magnesium, cools, forming an intensity maximum for Mg X at 0157 UT followed by a subsequent decline in Mg X emission as the material cools below 1.4×10^6 K. As the material continues to cool the O VI emission increases, reaching a maximum at about 0208, and then as the temperature falls below 3×10^5 K, the temperature at which O VI is the dominant oxygen ion, the O VI emission also declines. At the same time the emission in lines formed at cooler temperatures continues to increase. Since the O III line is still increasing in intensity at 0240 UT while the Ne VII line is decreasing in intensity, material is still draining out of the loops at 0240 UT. Since the Si XII emission is constant after 0224, no additional hot coronal material appears to be condensing out after 0224.

Levine and Withbroe (1976) estimated the total mass drained from the loops. As a first approximation the mean electron density derived from the Mg X emission is about 2×10^9 cm^{-3} and the total mass is about 3.4×10^{14} grams of which about 70% condenses and falls out of the loops. The dominant cooling mechanism appears to be radiation. Approximate radiative cooling times estimated from a simplified radiative cooling model using Cox and Tucker's (1959) radiative cooling rates, are in good agreement with the observed variation of the loop emission.

Models of one of the loops in the loop complex constructed by Levine and Withbroe (1976) yield the variation of intensity across the loop shown in Figure 2-4. These intensities were computed using equation (9) where I is the intensity, P is the pressure, and ρ is the distance from the axis of the loop.

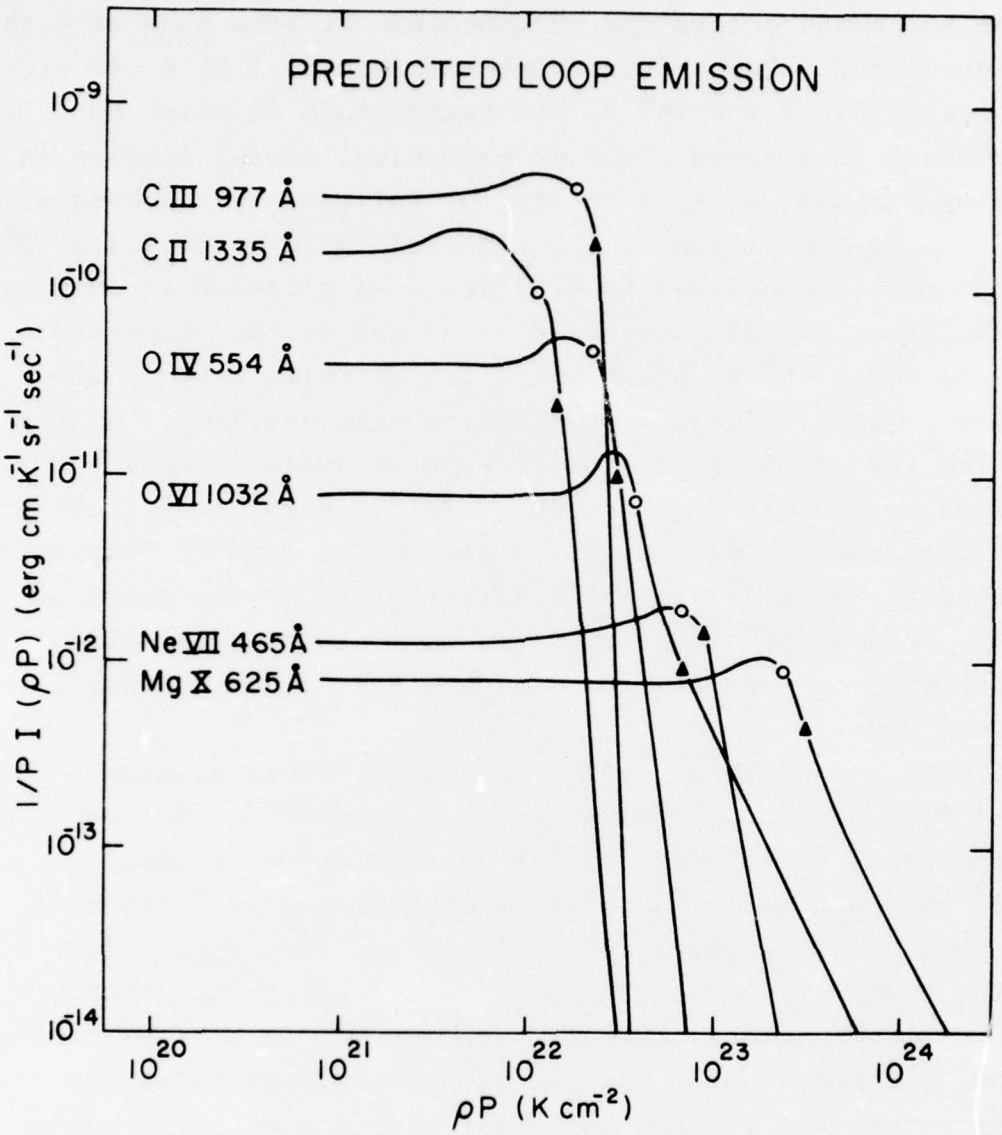

Figure 2-4. Results of model calculations for one position along the loop shown in Figure 2-3. The position is the one marked nearest the upper edge of the spectroheliogram and the observation time of the data used was 0152 UT. The value plotted is $I(\rho P)/P$ where I is the intensity of emission in the indicated spectral line that would be seen by an observer looking along a line of sight a distance ρ from the loop axis. The curve for each line is marked with a circle (triangle) at the value ρP indicating the outer edge of the volume where the integrated intensity reaches 75% (90%) of its total value.

Since the maximum observed radius ρ for the O VI λ 1032 line is 5 arc seconds the minimum pressure in the loop is about $P = n_e T = 2 \times 10^{15}$ for this loop. Because the radius of the Mg X emitting sheath calculated for typical loop models is so much larger than that of the cool cores (see Figure 2-4) it is likely that a number of cool cores will share a common hot envelope.

2.4 Conclusions

The behavior of the loop complex observed on 24 November, 1973, suggests that when the heating produced by the mechanism responsible for heating a coronal loop decreases sharply, the material in the loop will cool rapidly and fall into the chromosphere. The amount of material falling into the chromosphere can be fairly large, of the order of a few times 10^4 grams and can deposit the order of 10^{28} ergs when its gravitational potential energy is released. This energy is comparable with the total energy released by a small flare. The physical processes which cause the formation of active region loops are evidently very persistent, because further observations of McMath 12628 showed that within about 12 hours the loops studied fill with material again and assume a configuration similar to that before the event shown in Figure 2-1. A more detailed discussion of the event of 24 November 1973 is given by Levine and Withbroe (1976).

Events such as the one described above should produce significant changes in the radio emission observed at mm and cm wavelengths. Additional studies should be undertaken to determine how frequent such events are and what effect they have at radio and optical wavelengths accessible to ground-based instrumentation which monitor the sun on a more continuous basis than satellite experiments capable of observing the sun with high spatial resolution. High resolution XUV observations are needed to provide additional constraints on

loop models, particularly with regard to the dimensions of the cool cores. Observations with higher spatial resolution than currently available will provide data for generating better and more reliable models. High spectral resolution is also desired for measuring Doppler shifts and thereby observing more directly the flow of material along loops.

2.5 References

Levine, R.H. and Withbroe, G.L.: 1976, "Physics of an Active Active Region Loop System," Solar Phys., in press.

Pottasch, S.R.: 1964, "On the Interpretation of the Solar Ultraviolet Emission Line Spectrum," Space Sci. Rev., 3, 816.

Pottasch, S.R.: 1967, "The Inclusion of Dielectronic Recombination Processes in the Interpretation of the Solar Ultraviolet Spectrum," Bull. Astron. Inst. Neth., 19, 113.

Vaiana, G.S.: 1976, private communication.

Vorpahl, J.A.: 1976, private communication.

Withbroe, G.L.: 1970, "Solar XUV Limb Brightening Observations. I: The Lithium-Like Lines: Solar Phys. 11, 42.

Withbroe, G.L.: 1975, "The Analysis of XUV Emission Lines", Solar Phys. 45, 301.

3.0 THE 7 SEPTEMBER 1973 FLARE

3.1 Introduction

The 7 September, 1973 flare was one of the largest and best observed flares that occurred during the Skylab mission. It emitted strongly at radio, visible (Hα), EUV, and soft X-ray wavelengths and caused a disturbance in the corona, a large interplanetary shock wave at IAU and was associated with an increased proton level at the earth. For these reasons it is a significant flare to investigate. We summarize below some information about the 7 September flare derived from EUV observations of this event.

The 7 September, 1973 event consisted of a large double ribbon flare which occurred at W46 S18 in McMath region 12507. As observed in Hα the flare started at 1141 UT, reached maximum at 1212 and ended at 1342. The flare was accompanied by strong soft X-ray emission which started at about the same time as the Hα flare and peaked at 1207 UT. The soft X-ray flux did not return to preflare levels until sometime after 1700 UT. Radio activity observed near the time of the flare includes at metric wavelengths a type I noise storm from 1008 to 1537 UT, a type II burst from 1220 to 1222 UT, a type IV burst from 1235 to 1400 UT, and at 2800 MHZ an intense noise burst beginning at 1140 UT and rising precipitously at 1155 UT (cf. Gosling, et al., 1975; Solar Geophysical Data, 1974; Geophysical and Space Data Bulletin, 1973),

At 1307, in the first photograph acquired after the flare by the Skylab white light coronagraph, the corona above the western limb of the sun was unusually disturbed and chaotic as compared to coronal photographs obtained before the flare (Gosling, et al., 1975). Gosling, et al. attribute this to a coronal disturbance associated with a large dark surge produced by McMath region 12507 near the time of flare onset. They estimate a total ejected mass of 2.4×10^{16} grams with an energy content of 1.1×10^{32} ergs. These values are in reasonably good agreement with estimates for the mass and energy content of a large interplanetary shock wave disturbance detected at 1 AU. An increase in the proton count at the earth and a modest PCA are also attributed to the 7 September flare (Geophysical and Space Bulletin, 1973).

3.2 EUV Observations

The 7 September flare started during the night portion of the Skylab orbit and consequently the flare rise was not observed by the Skylab instrumentation. The first EUV observations acquired by the Harvard Skylab experiment were obtained at 1222 UT, about ten minutes after the Hα maximum when the 1 - 8 Å soft

X-ray flux was still near its maximum value (see Figure 3-1). High time resolution EUV observations consisting of one dimensional spectroheliograms were obtained from 1222 until 1248 UT. These one dimensional spectroheliograms, hereafter denoted as MLS (mirror line scan) observations, cover an area 5 arc seconds by 5 arc minutes with 5 arc second spatial resolution and 5.5 second time resolution. In the MLS mode intensities of Ly α λ 1216, C II λ 1335, C III λ 977, O IV λ 554, O VI λ 1032 and Mg X λ 625 were measured simultaneously with the photoelectric detection system of the instrument. During this time the EUV intensities decreased slowly, until the maximum intensities in all lines were about a factor of 2 to 3 lower at 1248 than they were at 1222.

At 1248 a set of 5 arc minute by 5 arc minute spectroheliograms was made in the same set of lines measured in the MLS mode. Four of these spectroheliograms are shown in Figure 3-2. At 1255 UT a wavelength scan from 1335 to 280 Å was obtained followed by a short period of observations in the MLS mode and then a second set of 5 arc minute by 5 arc minute spectroheliograms made simultaneously in each of the six spectral lines mentioned earlier. In subsequent orbits of Skylab spectroheliograms were obtained at 1408 and 1542 UT in these same spectral lines. Samples of these spectroheliograms are shown in Figures 3-3 and 3-4. Between 1419 and 1433 spectroheliograms were obtained in several other spectral lines in addition to the six lines given above.

In the present study we used only the Ly α, C II, C III, O IV, O VI, and Mg X spectroheliograms because of the more complete coverage in time for these lines. These data were supplemented by information obtained from the wavelength scan acquired at 1255 UT in a bright Hα area of the flare.

A comparison of the spectroheliograms in Figure 3-2 illustrates several important characteristics of flares than can be observed directly for the first time with simultaneous observations acquired with high spatial resolution in lines formed

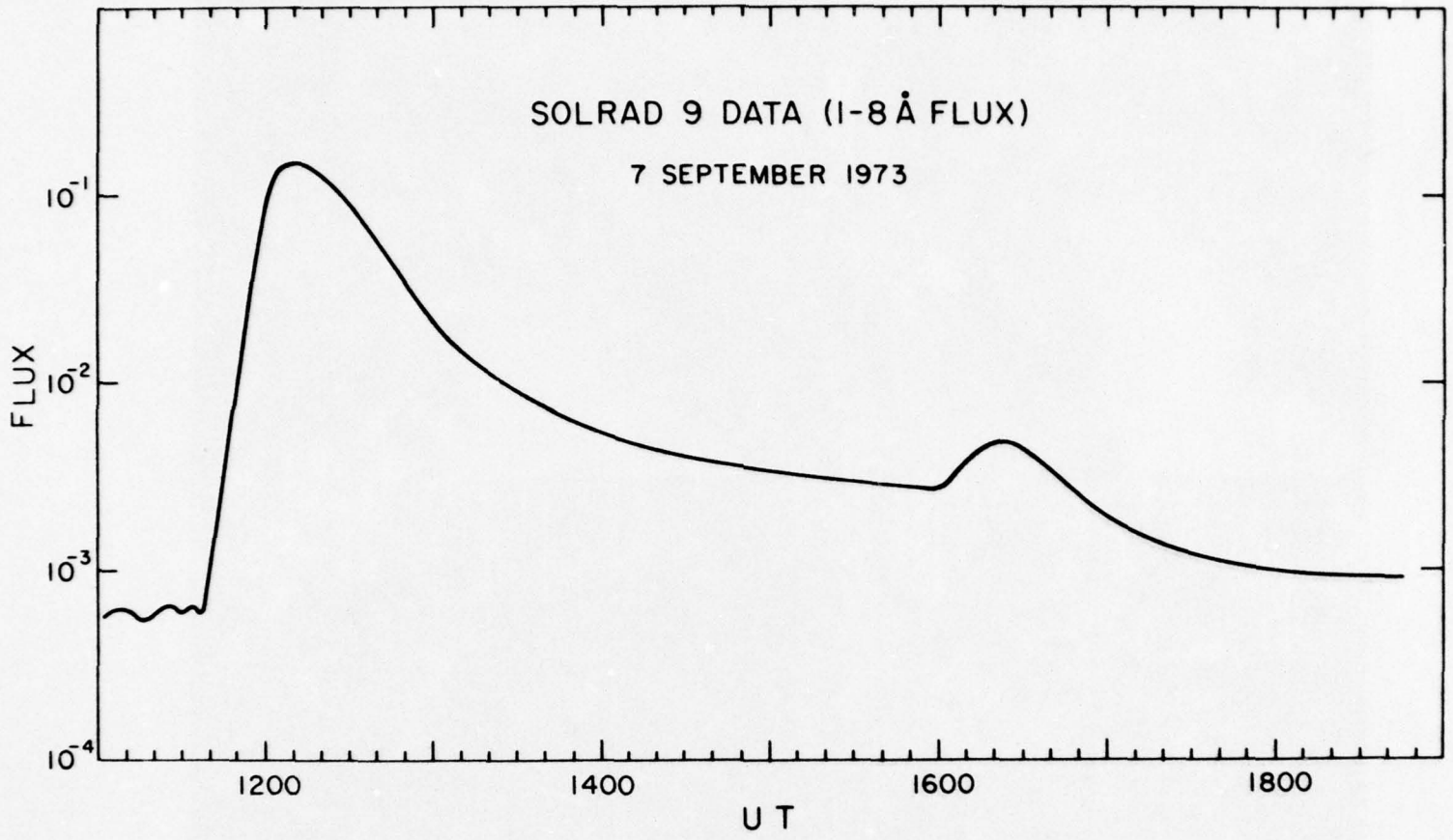

Figure 3-1. Smoothed data from Solrad 9.

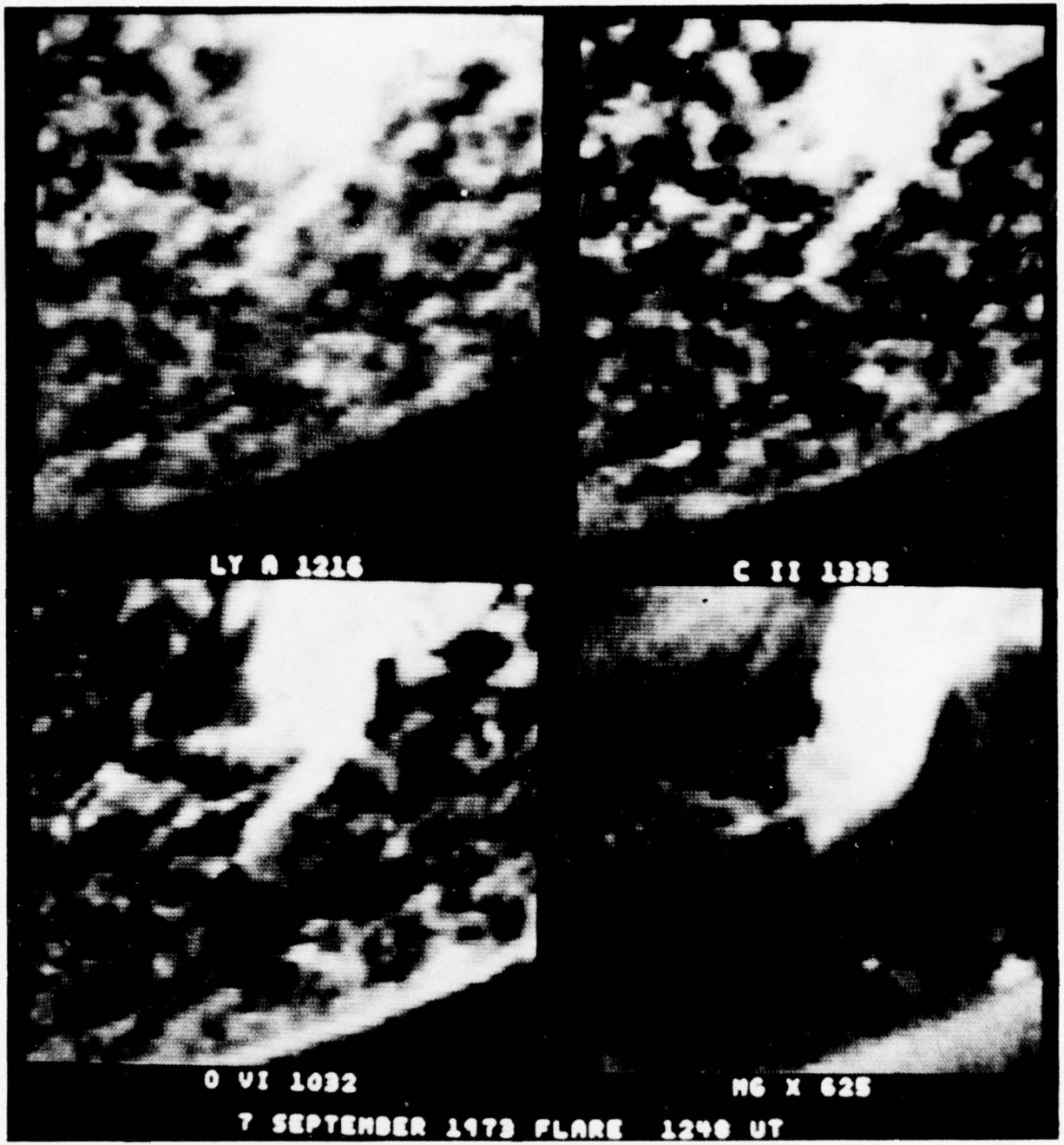

Figure 3-2. EUV spectroheliograms of McMath region 12507 at 1248 UT on 7 September, 1973.

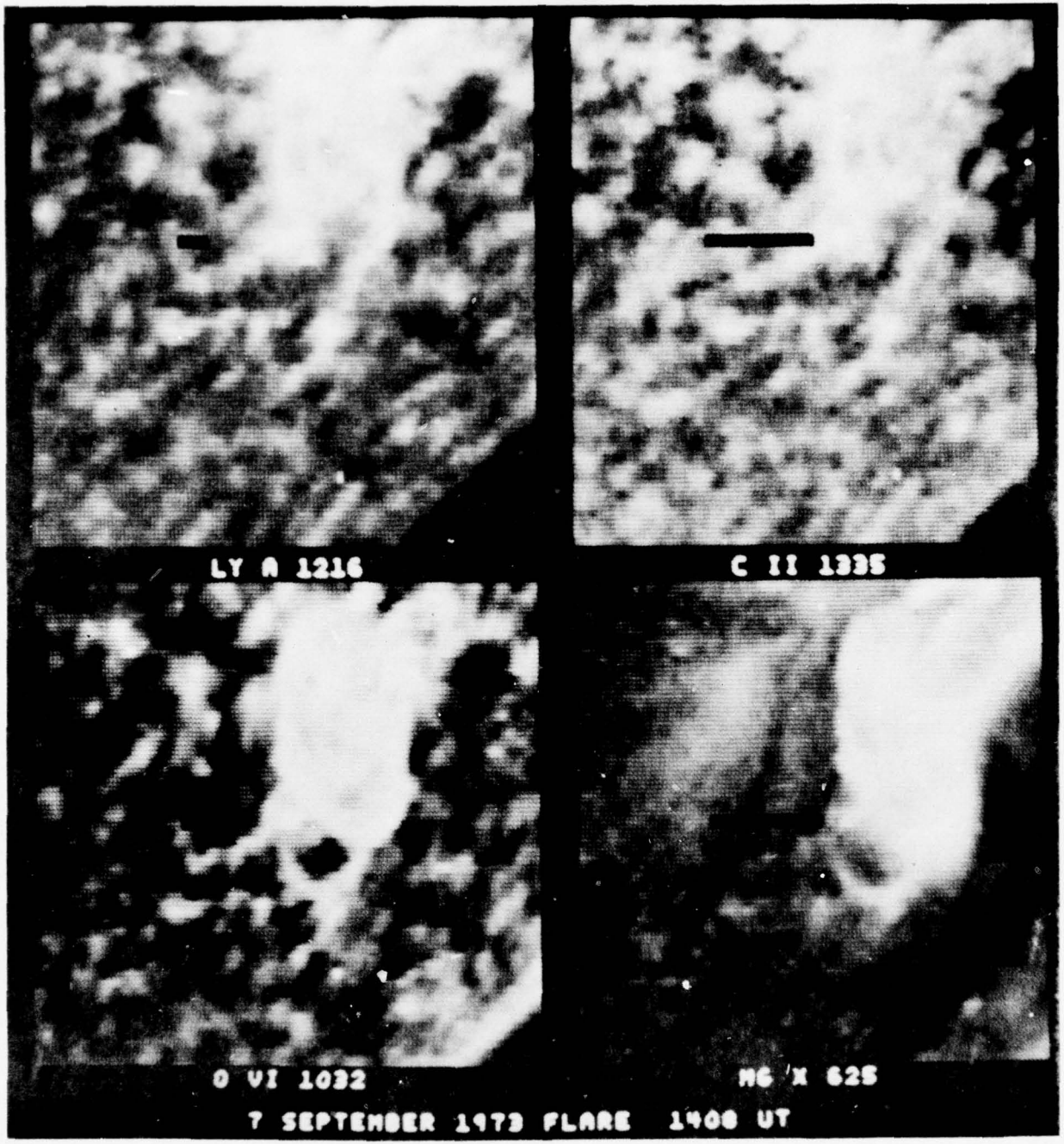

Figure 3-3. EUV spectroheliograms of McMath region 12507 at 1408 UT on 7 September, 1973.

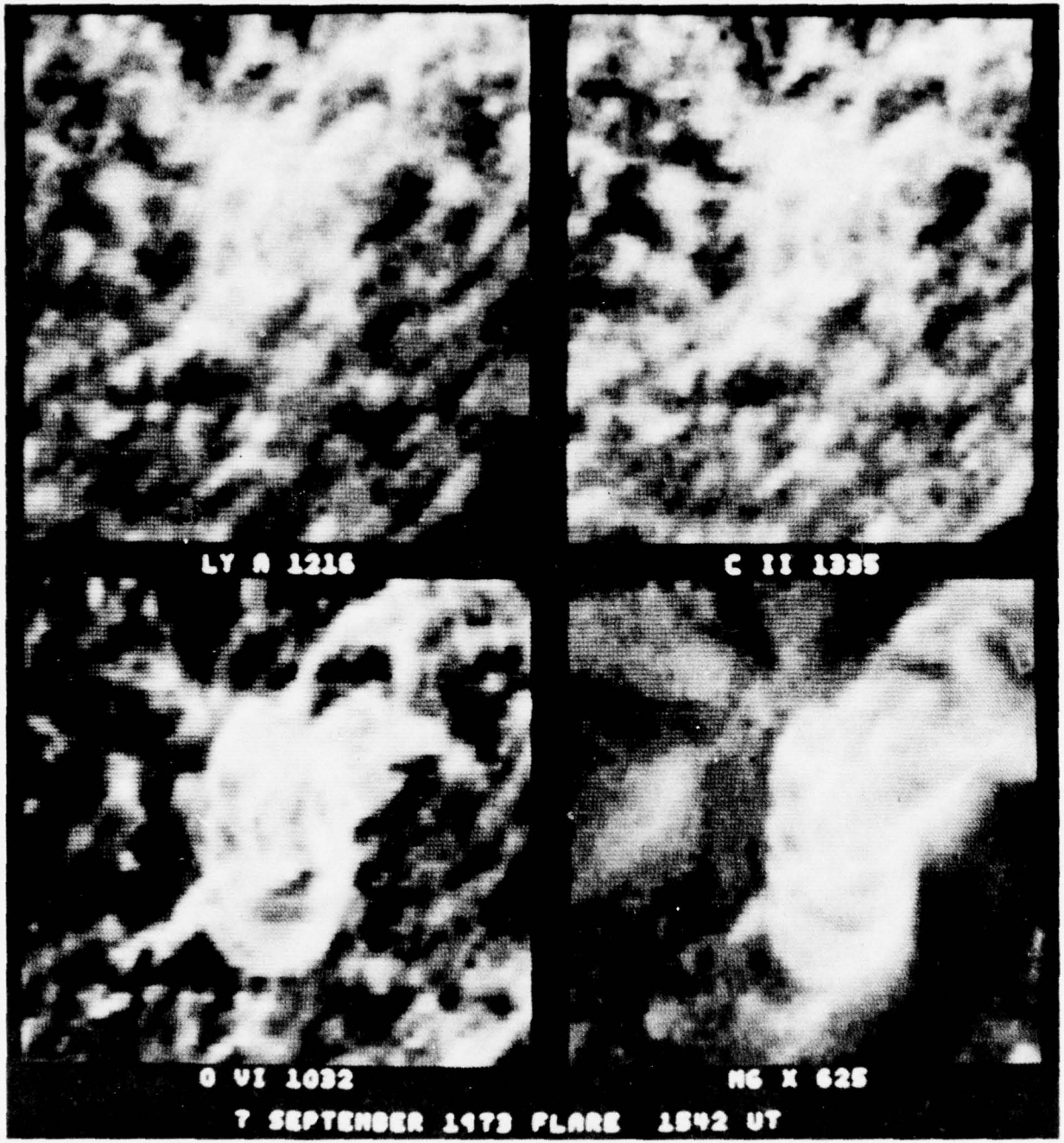

Figure 3-4. EUV spectroheliograms of McMath region 12507 at 1542 UT on 7 September, 1973.

in the chromosphere (Ly α), transition layer (C II and O VI), and corona (Mg X). In the coronal line Mg X λ 625 the flare consists of bright loops or arches, while in lines formed at lower temperatures (O VI, C II and Ly α) the brighter areas of the flare are located at the footpoints of the flare loops, although some loops are visible in O VI as well as Mg X. This suggests that the hot flare plasma is confined to magnetic loops and as it cools, it deposits energy in the chromosphere by conduction at the footpoints of the loops. In the analysis section below we will present estimates of the densities in the loops, radiative energy losses in these loops, the amount of energy conducted downward to the chromosphere and the energy radiated by Ly α in the upper chromosphere.

In the spectroheliograms obtained at later times the flare loops are larger, but fainter than at 1248 (for example, compare the Mg X spectroheliograms in Figures 3-2, 3-3, and 3-4). Since we do not have more frequent observations we cannot determine if the apparent increase in size is caused by an expansion of the loops or by adjacent higher loops becoming bright later in the flare. The Mg X loops are very similar in size and shape to flare loops observed with the Skylab soft X-ray experiment of American Science and Engineering. We are indebted to D. Rust of AS&E for supplying us with copies of the AS&E X-ray photographs of this flare.

3.3 Analysis

The EUV observations of the 7 September flare obtained by Skylab provides information about the physical conditions in the flare plasma during the declining phase when the hot plasma created by the initial event is cooling by radiation and by conduction to the lower layers of the atmosphere. The EUV data can be used to derive information about the temperatures, densities, and cooling rates of the flare plasma.

We consider first the wavelength scan obtained at 1255 UT, about 23 minutes after the Hα flare maximum when the soft X-ray emission was still relatively high (see Figure 3-1). This

spectrum was obtained in a 5 arc second by 5 arc second area at the footpoint of a bright flare loop (as seen in Mg X). From the intensities of the N V λ 1239, O VI λ 1032, Ne VIII λ 770 and λ 780, Na IX λ 682, Mg X λ 625, Al XI λ 550, Si XII λ 499, and Fe XVI λ 362 and λ 335 lines we derived the differential emission measure Q(T) as a function of temperature using the procedure outlined in Section 2.2. The resulting function Q(T), given in Figure 3-5, suggests that between log T = 5.4 and 6.4 the differential emission measure decreases slowly with increasing temperature, approximately as $T^{-1/2}$. At higher temperatures, log T $\geq$ 6.4 the differential emission measure increases with temperature until it reaches approximately the same value as it had at log T = 5.4.

From the differential emission measure one can obtain information about the electron pressure $P = n_e T$ in the flare loops. The volume occupied by the portion of the loop in the line of sight corresponds to approximately 5 arc seconds by 5 arc seconds by 30 arc seconds as estimated from the spectroheliograms obtained at 1248 and 1300 UT. If the hot flare plasma ($T \geq 10^6$ K) occupies most of this volume then the pressure in this volume is approximately $4 \times 10^{16} \lesssim P \lesssim 10^{17}$. The uncertainty in the pressure is caused by the uncertainty in the shape of the differential emission curve above log T = 6.4.

One can also estimate the total energy flux carried by conduction from the hot flare plasma to the upper chromosphere. If we assume that the flare loop has a temperature which monotonically increases with height and that the pressure in the transition layer between the hot flare plasma (where $T > 10^6$ K) and the cooler chromosphere is the same as the pressure estimated above for the hot flare plasma, then we can derive the conductive flux from the equation relating differential emission measure Q(T) with the conductive flux F_c. From Withbroe (1975)

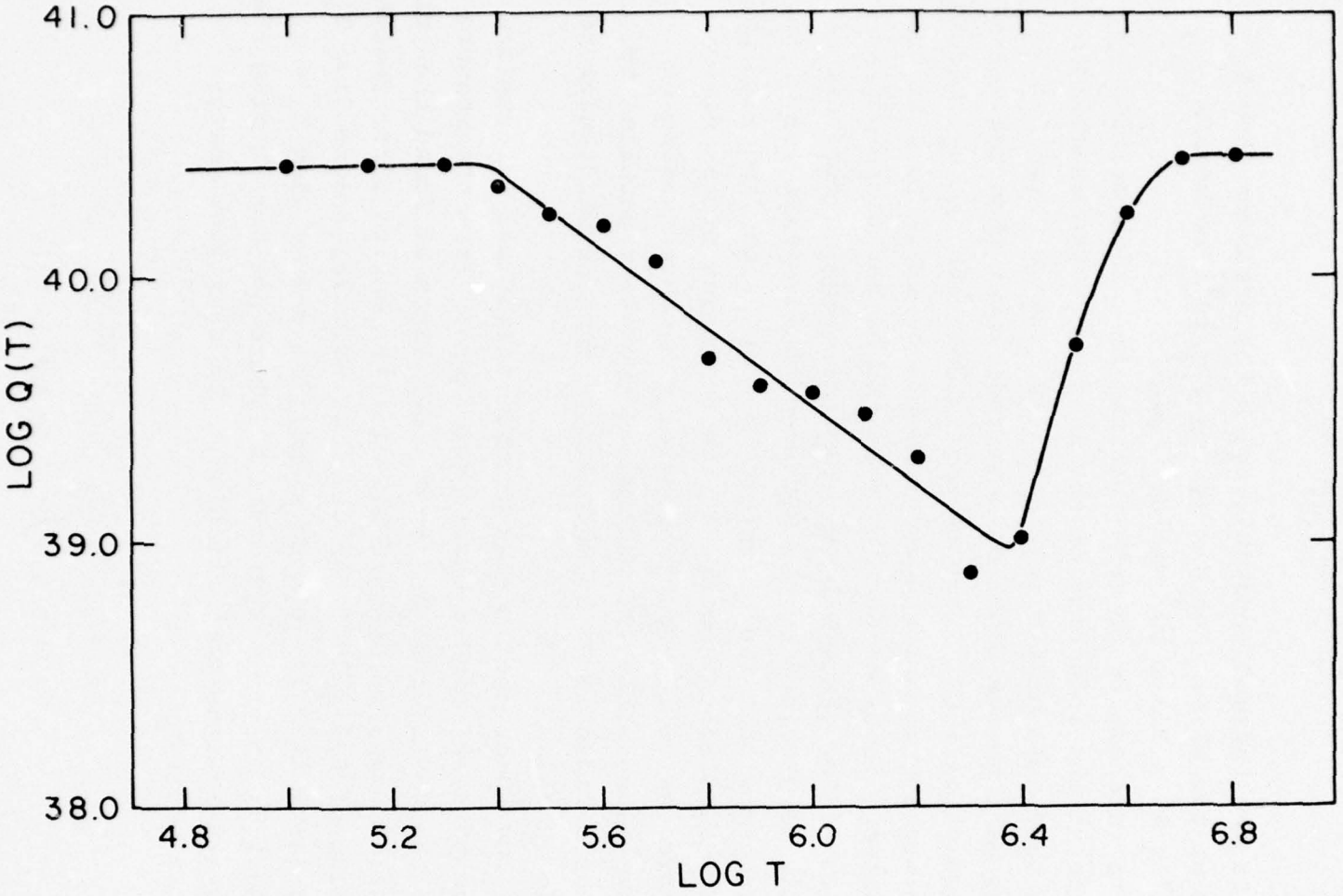

Figure 3-5. Differential emission measure for bright EUV and Hα emitting area in 7 September 1973 flare. The points are from the analysis procedure, the line is the best fit taking into account the "noise" introduced in the numerical analysis.

$$F_C = \frac{\kappa P^2 A_s T^{1/2}}{Q(T)} \qquad (10)$$

where κ is the thermal conductivity, P the pressure, and A_s the area of the slit. For $4 \times 10^{16} \lesssim P \lesssim 10^{17}$ we obtain $8.5 \times 10^6 \lesssim F_c \lesssim 5.3 \times 10^7$ erg cm^{-2} sec^{-1}.

It is interesting to note that the Ly α flux emitted by the region at the footpoint of the loop where the wavelength scan was made is approximately 3.7×10^6 erg cm^{-2} sec^{-1}, about one half to one order of magnitude lower than the estimated conductive flux. This is consistent with the hypothesis that the heating of the upper chromosphere, where Ly α is the major emitter, is by conduction from the hotter flare plasma located above the chromosphere. Further evidence for this hypothesis is provided by the EUV spectroheliograms (cf. Figure 3-2) which show that the brightest Ly α emission (and also the brightest Hα emission) occurs at the footpoint of the flare loops where one would expect the greatest concentration of conductive flux, since the thermal conductivity parallel to the magnetic field lines is much larger than perpendicular to the field lines.

The EUV spectroheliograms provide additional information about the physical conditions in the flare. From the measurements of the O VI λ 1032 and Mg X λ 625 lines we found that the differential emission measure Q(T) for the entire flare region has a value of 6.5×10^{41} for the O VI emitting volume ($\log T_1 = 5.5$) and 1.5×10^{42} for the Mg X emitting volume ($\log T_1 = 6.15$) where T_1 is the temperature at which the ion forming the line has its maximum concentration. The radiative energy losses are given by

$$F_r = \int n_e (n_H + n_p) \, Lr \, dV$$
$$= 0.8 \int n_e^2 \, L_r \, dV$$

for a fully ionized plasma of solar composition. The quantities n_H and n_p are the density of hydrogen atoms and protons and L_r is the radiative loss function.

From the definition of the differential emission measure Q(T) (see equation (3)) we obtain

$$F_r = 0.8 \int Q(T)\ L_r\ (T)\ dT. \qquad (12)$$

The radiative loss function L_r (T) has been computed by several investigators (cf. Cox and Tucker, 1959; Raymond, Cox, and Smith, 1976). If we assume that Q(T) has the form AT^B with the coefficients A and B defined by the values of Q(T) derived from the O VI and Mg X intensities, we find that the total radiative loss for the flare material with $T \geq 10^5$ K is about 10^{27} ergs per second at 1248 UT. Because of the uncertainty in the form of Q(T), particularly for high temperatures ($T \geq 2 \times 10^6$ K), the uncertainty in this value for the radiative losses is about one-half order of magnitude. In estimating the radiative losses we have assumed that there is no significant amount of flare material at temperatures greater than 10^7 K. This seems reasonable since the observations were obtained approximately one-half hour after flare maximum. There is still some material with temperatures of the order of 7×10^6 K since at 1248 the flare still can be seen in XUV spectroheliograms acquired by the NRL Skylab experiment in the Ca XVIII λ 345 line (Scherrer and Sandlin, 1976).

Intensities obtained from the O VI and Mg X spectroheliograms can also be used to estimate mean densities in the Mg X emitting volume of the flare plasma and to estimate the mean conductive flux. The mean intensity of the Mg X line in the flaring region is I = 4200 erg cm^{-2} sec^{-1} yielding a flux $4\pi IA = 6.8 \times 10^{21}$ erg sec^{-1} for each 5 arc second by 5 arc second resolution element which has an area of 3600 km by 3600 km. The mean electron density in the Mg X emitting volume can

be estimated from equation (1) under the assumption that the Mg X emission is coming from loops with diameters of the order of 5 arc seconds, as inferred from the dimensions of the loops observed in the spectroheliograms. From the observed mean flux we obtain an electron density $n_e = 1.5 \times 10^{10}$ cm^{-3}, which corersponds to $P = n_e T = 2.1 \times 10^{16}$. This is a lower limit to P, since the volume occupied by the Mg X emitting plasma in an average 5 arc second by 5 arc second pictal may be smaller than the assumed volume of 4.7×10^{25} cm^3 due to the presence of hotter material in the loops.

From the observed mean intensity of the O VI λ 1032 line, $I = 1.34 \times 10^4$ erg cm^{-2} sec^{-1}, the pressures computed from the Mg X line, and the differential emission meaasure derived for the entire flaring region from the O VI flux, we find a mean conductive flux of 1.1×10^7 erg cm^{-2} sec^{-1} for each 5 arc second by 5 arc second area in the flare which, when integrated over the total area of the flare, yields a total conductive energy loss of 3×10^{26} erg sec^{-1} at 1248 UT. The mean conductive flux calculated here is of the same order of magnitude as that derived earlier from the spectral scan. Because of the uncertainties in the assumed pressure and use of a mean conductive flux for each pictal in estimating the total conductive loss from the region, the value estimated for the latter is accurate to no better than one-half order of magnitude. The mean pressure of 2.1×10^{16} is somewhat lower than derived from the wavelength scan, as might be expected, since the Mg X intensities were averaged over both bright and faint loops while the spectral scan was obtained in a very bright loop.

It is interesting to note that the total Ly α energy radiated by the flaring region is approximately 10^{26} erg sec^{-1} at 1248, a value nearly the same as the total conductive loss estimate of 3×10^{26} erg sec^{-1}. As indicated earlier in the

discussion of the wavelength scan data, this provides evidence supporting the hypothesis that thermal conduction downward from the hot flare plasma is the source of the energy released by Ly α during the declining phase of the flare.

As indicated, the pressure estimated above from the Mg X flux emitted by the flaring region is a lower limit because of the averaging over the entire flaring area and the uncertainty as to the volume occupied by the Mg X emitting flare plasma in each pictal of the spectroheliogram. In the brightest areas of the flare loops observed at 1248 UT the intensity is approximately 2 times larger than the mean intensity averaged over the flare area, suggesting that the density in the Mg X emitting layer in the brightest flare loops is greater than or equal to 2.1×10^{10} cm^{-3} in these areas and $P = n_e T \gtrsim 3 \times 10^{16}$. Near flare maximum at 1222 UT when the first observations were obtained, the maximum Mg X intensity is approximately 6 times greater than the mean intensity at 1248 yielding a minimum density of 3.6×10^{10} cm^{-3} and $P \gtrsim 5 \times 10^{16}$.

At later times in the lifetime of the flare it is more difficult to estimate densities and radiative and conductive energy losses in the flare plasma. The difficulty is that the flare loops after 1400 UT no longer dominate the emission from the active region. Since we do not have observations before the flare occurred, we cannot separate out the non-flare background. At 1300 UT the EUV intensities are nearly the same as at 1248, only about 15% lower, hence the estimated densities, radiative losses and conductive losses at 1300 UT are nearly the same as at 1248. By 1408 the Mg X and O VI emission from the active region had fallen by a factor of 2.5 from the value at 1248 and at 1542 the intensities had fallen a factor of 3.5 below the values at 1248 UT.

3.4 Summary and Conclusions

The EUV observations of the 7 September, 1973, flare

indicate that both radiative and conductive cooling provide major energy losses for cooling the hot flare plasma. The location of the brightest Ly α emitting areas at the footpoints of the flare loops, as well as the order of magnitude agreement between the conductive energy losses and Ly α radiative losses, supports the hypothesis that conduction along the magnetic field lines is an important cooling mechanism (cf. Culhane, Veseky, and Phillips, 1970). Analysis of the Mg X data indicates that the electron density in the Mg X emitting volume of the flare loops exceeds 3.6×10^{10} cm^{-3} near the flare maximum and is equal to or greater than 2×10^{10} cm^{-3} one hour after flare maximum.

Much additional work can be done on the 7 September flare. Of particular value would be an analysis which utilizes all the Skylab EUV, XUV and soft X-ray measurements as well as radio data obtained from ground-based instrumentation to determine more precisely the temperatures and densities in the flare loops and to estimate more reliably the radiative and conductive energy losses as a function of time. The X-ray data are particularly important for evaluating the differential emission measure for that portion of the flare plasma with temperatures greater than 2×10^6 K. Other flares observed by Skylab should be similarly analyzed.

3.5 References

Cox, D.P. and Tucker, W.H.: 1969 "Ionization Equilibrium and Radiative Cooling of a Low-Density Plasma," Astrophys. J., 157, 1157.

Culhane, J.L., Vesecky, J.F. and Phillips, K.J.H.: 1970, "The Cooling of Flare Produced Plasmas in the Solar Corona", Solar Phys. 15, 394.

Geophysical and Space Data Bulletin: 1973, X, No. 3, Space Physics Laboratory, Air Force Cambridge Research Laboratories, L.G. Hanscom Field, Mass.

Gosling, J.T., Hildner, E., MacQueen, R.M., Munro, R.H., Poland, A.I., and Ross, C.L.: 1975, "Direct Observations of a Flare Related Coronal and Solar Wind Disturbance", Solar Phys., 40, 439.

Raymond, J.C., Cox, D.P., and Smith, B.W.: 1976, "Radiative Cooling of a Low-Density Plasma", Astrophys. J., 204, 290.

Scherrer, V.E. and Sandlin, G.D.: 1976, "Flare Atlas and Users Instruction Guide for NRL Flare Data 15 June, 5 and 7 September 1973", Naval Research Laboratory, Washington, D.C.

Solar-Geophysical Data, 1974 No. 355, U.S. Department of Commerce, Boulder, Colorado.

Withbroe, G.L.: 1975, "The Analysis of XUV Emission Lines", Solar Phys. 45, 301.

4.0 THE CHROMOSPHERIC MODEL

4.1 Introduction

The purpose of this work is to establish an empirical model of the solar atmosphere from approximately the temperature minimum of around 4200 K to the transition region at 15000 K. The model of the atmosphere provides the first link between the observational data and the physical description in terms of temperatures and densities. The basic model is necessary to study and describe a wide variety of phenomena that take place in the chromosphere.

In this report we summarize the results of the determination of the temperature structure of the middle chromosphere. A more detailed description is almost complete and will be shortly submitted for publication (Vernazza, Avrett, and Loeser, 1976b).

4.2 Model of the Photosphere and Temperature - Minimum Region

The study of the photosphere and temperature minimum region was completed and has already been published (Vernazza et al.,

1976a). In this work we present a non-LTE empirical model of the quiet photosphere. The model computed continuum intensities in the 0.15 to 500 μm range are in good agreement with the observations. We found that: (a) new absolute measurements in the 1 to 2μ region are needed to establish the structure of the deepest observable layers, (b) absolute measurements are needed in the 20 to 200μ regions to verify the temperature minimum temperature, (c) the far ultraviolet spectrum is formed in NLTE and studies of these spectra assuming LTE can be substantially in error, and (d) the line opacity could account for the ultraviolet "missing opacity".

4.3 Model for the Chromosphere

The details for the computational method have been described by Vernazza, Avrett and Loeser (1973). In summary, we solve the statistical equilibrium equations and the radiative transfer equations of the relevant lines and continuum for the following ions SiI, CI, H, He I and He II. We assume a plane parallel atmosphere in hydrostatic equilibrium.

The temperature distribution in the chromosphere is best determined from continuum observations in the range $200\mu < \lambda < 3$ cm and $0.04\ \mu m < \lambda < 0.16\mu m$. It can also be determined from line profiles of strong chromospheric lines or using eclipse observations. However, the complexities in the interpretation of eclipse observations and optically thick emission lines makes the temperature determinations based on these observations not as reliable as the one determined from continuum observations.

The temperature distribution was obtained by trial and error until the computed continuum intensities agreed with the observations. Of the continuum observations the ultraviolet continua contain the greatest amount of information about the chromosphere temperature distribution. Special care was taken to match these observations. In figure 4-1 we present the presently available observations of the sun's central intensity

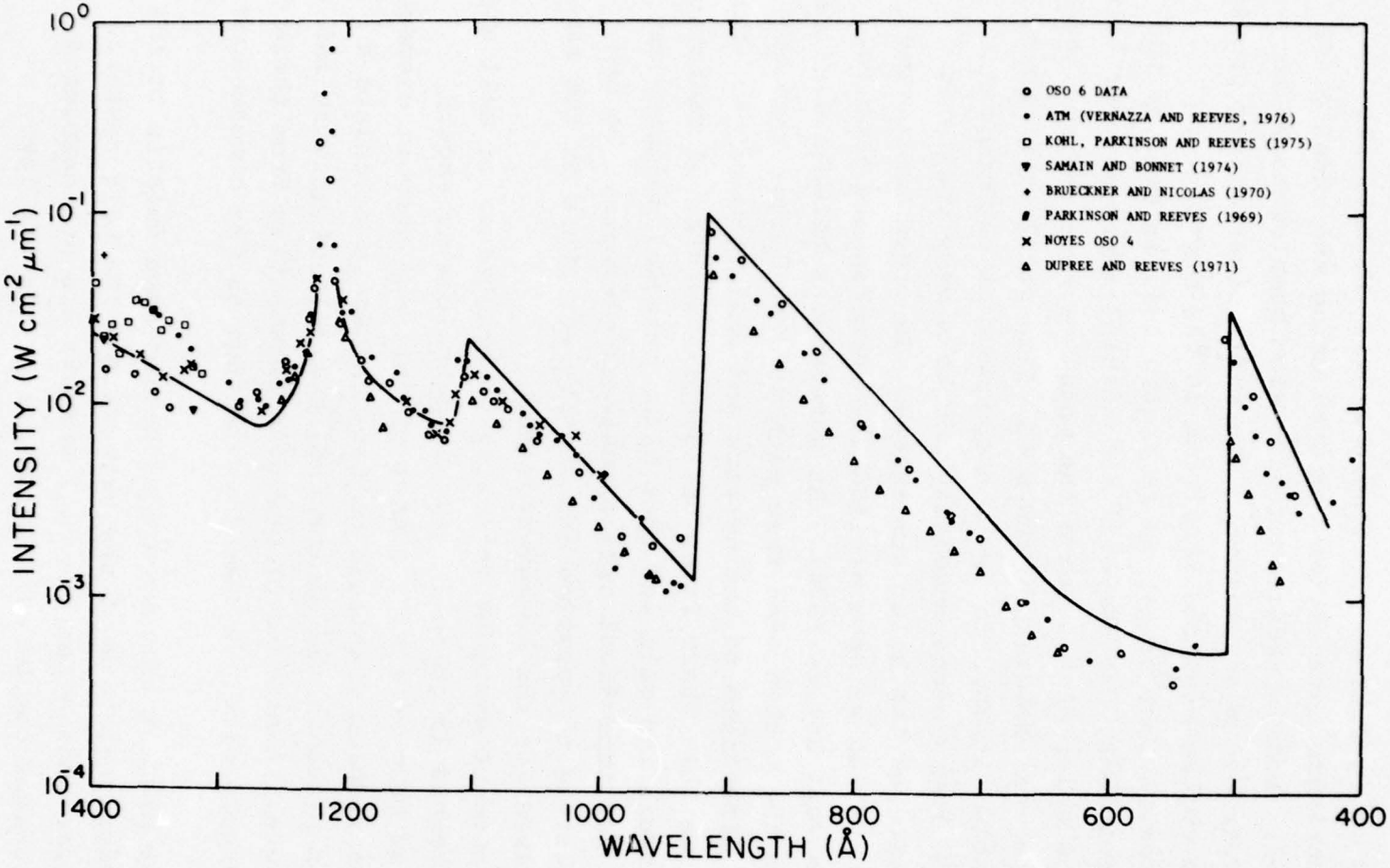

Figure 4-1. A comparison between the computed and observed intensities of the continua between 400 and 1400 Å. The points are the observations, the solid line the calculated intensities.

in the 0.04 μm to 0.16 μm wavelength range. We have also included continuum intensities computed using the model given in Table 4-1. Model predictions have also been compared to radio and infrared measurements. The radio observations provide constraints on the electron densities in the model.

The observations presented in Figure 4-1, as well as the radio observations, are temporal and spatial averages over large areas of the solar disk. Hence the model we have derived refers to a hypothetical homogenous sun with plane parallel geometry. Since the solar atmosphere is inhomogeneous at chromospheric heights, the homogeneous model may not be a very realistic representation of the solar atmosphere. In order to improve the representation we have divided the chromosphere into cell and network (cf. Reeves 1976). At wavelengths between 0.04 μm and 0.16 μm the photon mean free path is much larger than the horizontal dimensions of the network and cell structures. Thus we can assume that there is no horizontal transfer of radiation between network and cell and that plane parallel geometry can be adopted for individual cell or network elements. We can then calculate a temperature and density structure in the same manner as used for the homogeneous model.

The range of emergent intensity or brightness of cell and network elements is quite large. In principle we should calculate as many models as number of cell and network elements. To keep the problem tractable we have chosen to calculate 4 models as representative of the entire sample of network and cell elements. A mixture of computed intensities from these 4 models should give the same results then as the homogeneous model.

At the present time we are adjusting some details of the 4 models representative of the network and the cell centers. Although some models for the cell centers are not completed some conclusions can be already be drawn. In the low

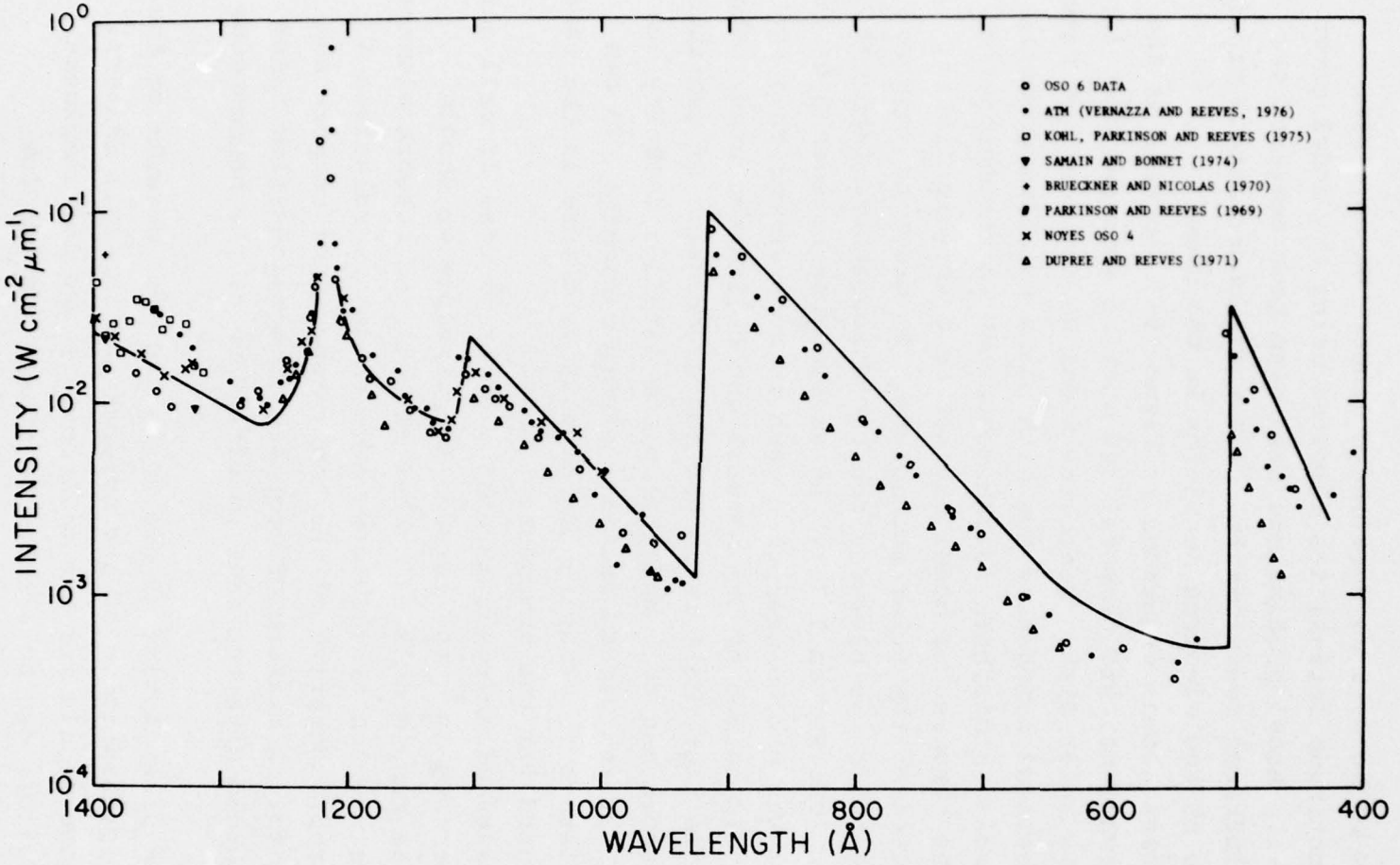

Figure 4-1. A comparison between the computed and observed intensities of the continua between 400 and 1400 Å. The points are the observations, the solid line the calculated intensities.

Table 4-1. HOMOGENEOUS CHROMOSPHERIC MODEL

Z (km)	τ_{5000}	ELECTRON TEMPERATURE (K)	VELOCITY (km/s)	TOTAL HYDROGEN DENSITY (cm^{-3})	ELECTRON DENSITY (cm^{-3})	TOTAL PRESSURE (dyne/cm^{-3})	TURBULENT PRESSURE FRACTION
-2149	2.018E-06	4.700E+04	1.420E+01	1.263E+10	1.399E+10	2.107E-01	1.414E-01
-2148	2.019E-06	3.900E+04	1.420E+01	1.482E+10	1.636E+10	2.108E-01	1.658E-01
-2147	2.020E-06	3.300E-04	1.415E+01	1.706E+10	1.875E+10	2.109E-01	1.894E-01
-2145	2.023E-06	2.900E+04	1.410E+01	1.904E+10	2.074E+10	2.111E-01	2.096E-01
-2142	2.027E-06	2.500E+04	1.410E+01	2.150E+10	2.316E+10	2.115E-01	2.363E-01
-2140	2.030E-06	2.400E+04	1.400E+01	2.232E+10	2.393E+10	2.118E-01	2.415E-01
-2127	2.052E-06	2.300E+04	1.340E+01	2.382E+10	2.537E+10	2.137E-01	2.340E-01
-2107	2.087E-06	2.260E+04	1.250E+01	2.529E+10	2.689E+10	2.169E-01	2.130E-01
-2077	2.143E-06	2.240E+04	1.170E+01	2.678E+10	2.844E+10	2.219E-01	1.932E-01
-2037	2.222E-06	2.220E+04	1.050E+01	2.897E+10	3.069E+10	2.290E-01	1.630E-01
-1977	2.352E-06	2.200E+04	9.400E+00	3.179E+10	3.348E+10	2.407E-01	1.364E-01
-1967	2.375E-06	2.150E+04	9.300E+00	3.287E+10	3.445E+10	2.428E-01	1.369E-01
-1965.5	2.379E-06	1.970E+04	9.250E+00	3.580E+10	3.684E+10	2.431E-01	1.473E-01
-1964	2.382E-06	1.750E+04	9.200E+00	4.019E+10	4.011E+10	2.435E-01	1.634E-01
-1962	2.388E-06	1.460E+04	9.150E+00	4.781E+10	4.527E+10	2.441E-01	1.918E-01
-1960	2.395E-06	1.230E+04	9.100E+00	5.620E+10	5.025E+10	2.447E-01	2.224E-01
-1958.5	2.401E-06	1.070E+04	8.950E+00	6.443E+10	5.434E+10	2.453E-01	2.460E-01
-1957	2.407E-06	9.000E+03	8.900E+00	7.537E+10	5.887E+10	2.459E-01	2.838E-01
-1944	2.461E-06	8.550E+03	8.700E+00	8.395E+10	5.877E+10	2.526E-01	2.941E-01
-1930	2.520E-06	8.300E+03	8.500E+00	9.278E+10	5.702E+10	2.607E-01	3.007E-01
-1900	2.637E-06	7.800E+03	8.000E+00	1.156E+11	5.320E+10	2.808E-01	3.082E-01
-1825	2.864E-06	7.160E+03	7.400E+00	1.844E+11	3.370E+10	3.519E-01	3.355E-01
-1735	3.033E-06	6.850E+03	6.700E+00	2.997E+11	2.110E+10	4.890E-01	3.217E-01
-1660	3.133E-06	6.690E+03	6.600E+00	4.436E+11	1.668E+10	6.655E-01	2.996E-01
-1575	3.238E-06	6.580E+03	5.600E+00	7.004E+11	1.657E+10	9.716E-01	2.643E-01
-1475	3.379E-06	6.480E+03	4.900E+00	1.230E+12	1.985E+10	1.573E+00	2.195E-01
-1375	3.576E-06	6.400E+03	4.100E+00	2.251E+12	2.631E+10	2.653E+00	1.667E-01
-1275	3.885E-06	6.280E+03	3.400E+00	4.262E+12	3.634E+10	4.672E+00	1.233E-01
-1200	4.258E-06	6.200E+03	3.000E+00	6.948E+12	4.719E+10	7.313E+00	9.998E-02
-1075	5.477E-06	6.030E+03	2.300E+00	1.642E+13	7.248E+10	1.611E+01	6.304E-02
-975	7.687E-06	5.870E+03	1.850E+00	3.373E+13	9.449E+10	3.149E+01	4.286E-02
-900	1.076E-05	5.680E+03	1.550E+00	5.982E+13	9.948E+10	5.336E+01	3.149E-02
-850	1.371E-05	5.540E+03	1.400E+00	8.889E+13	9.297E+10	7.689E+01	2.649E-02
-750	2.244E-05	5.150E+03	1.250E+00	2.074E+14	7.108E+10	1.661E+02	2.282E-02
-700	2.934E-05	4.890E+03	1.200E+00	3.299E+14	6.897E+10	2.505E+02	2.217E-02
-650	4.118E-05	4.625E+03	1.200E+00	5.377E+14	7.821E+10	3.867E+02	2.341E-02
-600	6.698E-05	4.390E+03	1.100E+00	8.985E+14	1.050E+11	6.117E+02	2.078E-02
-550	1.363E-04	4.190E+03	1.050E+00	1.529E+15	1.516E+11	9.927E+02	1.986E-02
-500	3.229E-04	4.150E+03	1.000E+00	2.545E+15	2.265E+11	1.633E+03	1.821E-02
-450	7.856E-04	4.200E+03	1.000E+00	4.138E+15	3.496E+11	2.688E+03	1.800E-02
-350	4.321E-03	4.460E+03	1.000E+00	1.022E+16	9.031E+11	7.041E+03	1.697E-02
-250	2.171E-02	4.750E+03	1.000E+00	2.371E+16	2.300E+12	1.738E+04	1.595E-02
-150	9.892E-02	5.120E+03	1.000E+00	5.124E+16	5.829E+12	4.044E+03	1.481E-02
-100	2.026E-01	5.445E+03	1.000E+00	7.159E+16	1.011E+13	6.003E+04	1.394E-02
-50	4.204E-01	5.840E+03	1.000E+00	9.671E+16	2.078E+13	8.691E+04	1.301E-02

chromosphere the network is between 1.5 and 3 times more dense than the cells in layers with the same temperature. In order to construct these models we have obtained average ATM spectra for network and cell areas. From these spectra we find that the observed Lyman continuum color temperature, which is indicative of the temperature of formation of the Lyman continuum, is larger in the network than in the cells. This implies that because the network is denser than cells, optical depth unity is reached at higher temperatures in the network.

It is also interesting to compare the Lyman continuum with the He I continuum. The observed ratio network vs. cell at the head of the Lyman continuum (912 Å) is 1.5 and the He I continuum (504 Å) is 2.0. These continua are formed at approximately the same physical regions. If the mechanism of formation of the Lyman continuum and the He I continuum were the same, the observed ratio network vs. cell should be approximately equal. The Lyman continuum is formed by collisions from the ground state, thus the intensity depends on the electron density. The He I continuum is formed by photoionization by corona-transition region radiation (Avrett et al., 1976). The intensity of the coronal lines is approximately the same in network as in cells, but the transition region lines are 2 to 4 times more intense in the network than in cells. The He I continuum should in part follow the transition line intensities, and therefore have a larger network/cell ratio than the Lyman continuum. The observations confirm the calculations showing that the He I continuum is formed by photoionization due to radiation from the transition region and corona.

The concept of using a set of models to represent typical elements of the chromosphere is a very useful one. For example, not every quiet area is exactly alike and therefore a different mixture of models may be necessary to represent different regions. Also, there is preliminary evidence suggesting that at chromospheric heights there is little difference between

normal quiet areas and coronal holes, the major exception being that the relative proportion of network and cell elements is different. Thus, since we already have models for individual cells and network, we will only need to change the mixture of individual element models to obtain a model representative of the chromospheric layer of coronal holes.

4.4 Conclusions

A homogeneous model for the photosphere, temperature-minimum region and chromosphere has been developed. The details of the model and its derivation are given in several papers by Vernazza et al. (1973, 1976a, 1976b). In order to represent the inhomogeneities in the chromosphere, four models for cell and network elements have been derived (Vernazza et al. 1976b). It is anticipated that the latter models may also be utilized to develop an inhomogeneous model for the chromospheric layer of coronal holes.

The major additional factor to be taken into consideration in developing future chromospheric models is the spicular component which represents an additional level of inhomogeneity beyond that incorporated in the Vernazza et al. model. It is highly desirable that EUV observations made with high spatial resolution, one arc second or better, be acquired in order to facilitate the development of reliable spicule models.

4.5 References

Avrett, E.H., Vernazza, J.E., and Linsky, J.L. 1976, "Excitation and Ionization of Helium in the Solar Atmosphere", Astrophys. J., in press.

Reeves, E.M. 1976, "The EUV Chromospheric Network in the Quiet Sun", Solar Phys., in press.

Vernazza, J.E., Avrett, E.H. and Loeser, R. 1973, "Structure of the Solar Chromosphere. I. Basic Computations and Summary of Results", Astrophys. J. 184, 605.

Vernazza, J.E., Avrett, E.M. and Loeser, R. 1976a, "Structure of the Solar Chromosphere. II. The Underlying Photosphere and Temperature-Minimum Region", Astrophys. J. Suppl. 30, 1.

Vernazza, J.E., Avrett, E.H. and Loeser, R. 1976b, "Structure of the Solar Chromosphere. III. The Chromosphere", to be submitted to Astrophys. J.

5.0 STUDIES OF CORONAL HOLES

5.1 Introduction

Some preliminary work on coronal holes was performed during the past year. These studies utilized extreme ultraviolet observations acquired by ATM as well as radio measurements acquired at several ground-based observatories. The purpose of these studies was to investigate the mean temperatures and densities in the upper transition layer and lower corona in several coronal holes.

Coronal holes are areas on the sun where the coronal temperature and density are lower than the surrounding quiet areas and active regions. Since the magnetic field in coronal holes is open, the solar wind can originate from these regions. It is the latter factor that has generated considerable interest in these features. There is a growing body of evidence that coronal holes are a major source of the solar wind, that many recurrent high speed solar wind streams originate in coronal holes and that coronal holes are responsible for recurrent geomagnetic disturbances (e.g. Krieger, et al., 1974; Neupert and Pizzo, 1974; Bell and Noci, 1975; Nolte, et al., 1975; Sheeley, et al., 1976). We summarize below results of two studies, one of a polar coronal hole for which preliminary results have been reported by Mariska (1976) and the other, of an equatorial coronal hole (Dulk, Sheridan, Smerd and Withbroe, 1976).

5.2 Observations

The EUV observations used in the studies were obtained by the Harvard experiment on ATM and have a spatial resolution of 5 arc seconds. The radio observations consist of brightness temperatures measured at 80, 160, 1420, and 10700 mhz. The radio measurements have angular resolutions of 3.8, 1.9, 3, and 1.25 arc minutes at respectively 80, 160, 1420, and 10700 mhz. For the polar hole the investigations utilized EUV emission gradients derived from the lines O VI λ 1032, Ne VIII λ 770, Mg X λ 625, Al XI λ 550, and Si XII λ 521. The observations were acquired at the north pole on 14 August, 1973. The study of the equatorial hole was based on radio measurements at the frequencies given above and EUV measurements in Mg X λ 625 and O VI λ 1032. The observations were acquired in July and August, 1973.

5.3 The Polar Coronal Hole

The intensities of the O VI, Ne VIII, Mg X, Al XI, and Si XII lines were analyzed by Mariska using the emission measure analysis technique developed by Withbroe (1975). The analysis indicates that low in the coronal hole (at a solar radius of 1.05 $R_\odot$) a large amount of material is at temperature of about 800,000 K with additional material at higher temperatures typical of the quiet sun. The temperature of the hotter material is difficult to determine by the emission measure technique because of the unavailability of high temperature lines in the data sample. At distances further above the limb 1.05 $R_\odot$ the percentage of cool material ($8 \times 10^5 \lesssim T \lesssim 10^6$ K) decreases.

In order to obtain more detailed information than provided by the emission measure analysis, the absolute intensities and emission gradients of the ultraviolet lines were analyzed using a simple two-component model in which the coronal hole is assumed to be homogeneous, in hydrostatic equilibrium with an isothermal corona and to have a transition layer in which the

temperature gradient is derived under the assumption of constant conductive flux. The quiet corona in front of and behind the coronal hole was assumed to be homogeneous, isothermal, and in hydrostatic equilibrium. The best fit to the data indicates that the density in the coronal holes at r = 1.03 $R_\odot$ is 2 x 10^8, the conductive flux is 6 x 10^4 erg cm^{-2} sec^{-1} and the coronal temperature is 10^6 K reached at about 1.08 $R_\odot$. For the quiet sun the adopted temperature was 2 x 10^6 K. The temperature gradient found for the coronal hole is approximately an order of magnitude below the quiet sun value.

5.4 Equatorial Coronal Hole

The analysis of the equatorial coronal hole by Dulk, et al. (1976) indicates that there appears to be a discrepancy between coronal hole models developed from EUV data and those developed from radio data. A given model predicts either higher radio brightness temperatures than observed or lower EUV line intensities than are observed. This discrepancy is caused by the different densities needed to explain the two types of measurements. The EUV data suggest that the density at the base of the transition region (where T = 10^5 K) corresponds to $\log n_e = 9.5 \pm 0.1$ with a conductive flux in the transition region of 1.1 x 10^5 erg cm^{-2} sec^{-1} while the radio data suggest $\log n_e = 9.0 \pm 0.1$ and a conductive flux $\leq$ 4.4 x 10^5 erg cm^{-2} sec^{-1}. Dulk et al. (1976) suggest several possible explanations for the discrepancy and indicate that more sophisticated models which involve mass flow, non-equilibrium ionization and thermal diffusion seem to offer the greatest hope of reconciling the EUV and radio observations.

5.5 Conclusions

The studies summarized above as well as other investigations currently being performed by various groups indicate that much additional work has to be done on coronal holes before we can reliably determine the physical conditions in coronal holes and

fully understand why these regions are sources of high speed solar wind streams. Currently available coronal hole models are generally homogeneous, plane-parallel models which assume hydrostatic equilibrium. Although these simple models provide a useful starting point for investigating physical conditions in coronal holes, much more sophisticated inhomogeneous, non-equilibrium models will be required to explain the variety of phenomena and features associated with coronal holes.

5.6 References

Bell, B. and Noci, G.: 1975, "Intensity of the Fe XV Emission Line Corona, the Level of Geomagnetic Activity, and the Velocity of the Solar Wind", submitted to Geophys. Res.

Dulk, G.A., Sheridan, K.V., Smerd, S., and Withbroe, G.L.: 1976, "Radio and EUV Observations of a Coronal Hole", submitted to Solar Phys.

Krieger, A.S., Timothy, A.F., and Roelof, E.C.: 1973, "A Coronal Hole and Its Identification as the Source of a High Velocity Solar Wind Stream", Solar Phys. 29, 505.

Krieger, A.S., Timothy, A.F., Vaiana, G.S., Lazarus, A.J., and Sullivan, J.D.: 1974, X-Ray Observations of Coronal Holes and Their Relation to High Velocity Solar Wind Streams", Solar Wind Three (C.T. Russell, ed.), Institute of Geophysics and Planetary Physics, University of California, Los Angeles, CA, p. 132.

Mariska, J.T.: 1975, "Extreme Ultraviolet Observations of a Polar Coronal Hole", Bull. Amer. Astron. Soc. 8, 338.

Neupert, W.M. and Pizzo, V.: 1974, "Solar Coronal Holes as Sources of Recurrent Geomagnetic Disturbances", J. Geophys. Res. 79, 3701.

Nolte, J.T., Krieger, A.S., Timothy, A.F., Gold, R.E., Roelof, E.C., Vaiana, G., Lazarus, A.J., Sullivan, J.D., and McIntosh, P.S.: 1976, "Coronal Holes as Sources of the Solar Wind", submitted to Solar Phys.

Sheeley, N.R., Jr., Harvey, J.W., and Feldman, W.C.: 1976, "Coronal Holes, Solar Wind Streams and Recurrent Geomagnetic Disturbances: 1973-1976", submitted to Solar Phys.

6.0 ACTIVE REGION FLARE RATES AND 8.6mm BRIGHTNESS TEMPERATURES

6.1 Introduction

Several investigations have provided evidence that there is a relationship between the rate of flaring of active regions and the intensity of the microwave radiation emitted by these regions. For example Kundu (1959), Pick-Gutmann (1961), and Tanaka and Kakinuma (1964) found that the flare productivity of active regions is correlated with their 3.2 cm brightness, while White (1972) and White and Mayfield (1973, 1975) found a correlation between flare productivity and the peak enhancement of the antenna temperature measured at 3.3 mm. The purpose of the present study was to investigate the relationship between the rate of flaring and the 8.6 mm brightness temperature of active regions through use of observations of 116 regions. The results of the study are given in two scientific reports (Withbroe and Vernazza, 1974, 1975) and a paper (Withbroe and Vernazza, 1976). We summarize these results below.

6.2 Observations

The 8.6 mm brightness temperatures used in the investigation were obtained from daily radio maps produced by the Air Force Cambridge Research Laboratories (AFCRL) radio telescope located in Waltham, Massachusetts (Kalaghan and Telford, 1970) and the radio telescope of the La Posta Astrophysical Observatory, Campo, California. The half-power beam widths of the AFCRL and La Posta telescopes at 8.6 mm are respectively 4.2 arc min and 2.8 arc min. The antenna temperatures given in the 8.6 mm radio maps were placed on an absolute brightness temperature scale by assuming the average quiet sun has a brightness temperature of 8300 K at 8.6 mm (Vernazza et al., 1973). The procedure

used in defining the quiet sun is given in the scientific reports (Withbroe and Vernazza, 1974, 1975). Information on solar flares was obtained from Solar Geophysical Data reports of the National Geophysical and Solar-Terrestrial Data Center, Boulder, Colorado. The observations utilized were acquired during the years 1969 to 1974.

6.3 Analysis

Only well-defined active regions were selected for study. A total of 106 regions were analyzed using AFCRL data from 1969 - 1973 and 10 regions using La Posta data from 1974. Because of the low spatial resolution of the 8.6 mm observations, the relationship between the rate of flaring and brightness temperatures of individual active regions was determined only during the time that the regions were within several days of central meridian passage. This was done so as to avoid the necessity of correcting for foreshortening of active regions when they were close to the limb and the associated difficulty of determining the relative contributions of individual regions to the observed brightness temperature measured near the limb.

The relationship between 8.6 mm brightness temperature and flare rate was derived in the following manner. The temperature range 8500 K to 11125 K was divided into 21 intervals with widths of 125 K. For each active region the 8.6 mm brightness temperature was plotted as a function of time. From these plots we determined the length of time the brightness temperature was within each 125 K temperature interval. Then the flare reports and observed relationship between brightness temperature and time were used to determine the number of flares and subflares that occurred in each brightness temperature interval.

The results of the AFCRL data are summarized in Table 6-1 which gives for each brightness temperature interval the total number of hours accumulated for the 106 active regions analyzed and the numbers of subflares, confirmed flares of importance $\geq$ 1, and confirmed flares of importance $\geq$ 2. For subflares we

Table 6-1. Number of flares and times associated with each 8.6 mm brightness temperature interval.

Brightness Temperature (K)	Hours	Number of Events		
		Subflares	(Imp. $\geq$ 1)	(Imp. $\geq$ 2)
8500	522	81	1	0
8625	1505	267	8	1
8750	1489	264	12	1
8875	1030	273	17	1
9000	773	219	30	3
9125	510	182	18	0
9250	304	111	12	1
9375	298	157	15	0
9500	339	196	24	2
9625	189	96	11	4
9750	95	53	3	1
9875	72	30	1	1
10000	63	29	4	2
10125	21	6	0	0
10250	27	4	2	1
10375	25	6	2	1
10500	11	7	0	0
10625	10.5	3	1	1
10750	7.5	5	0	0
10875	7.5	7	1	1
11000	2.0	1	0	0

used both confirmed and unconfirmed events. The ratio of the number of confirmed subflares and number of unconfirmed subflares is 1.2 for the regions studied. Data for individual regions are tabulated in reports by Withbroe and Vernazza (1974, 1975).

From the data in Table 6-1 mean flare rates were determined as a function of brightness temperature. Because of the small number of flares in many of the temperature intervals, the data were smoothed by expanding the width of each temperature interval from 125 K to 375 K when the flare rates were determined. The results, presented in Figure 6-1, indicate, as might be expected, that as the 8.6 mm brightness temperature of an active region increases, a larger proportion of the energy released by the region in the form of flares is contained in progressively larger flares. At all temperatures subflares are the most frequent event, particularly at low temperatures. At intermediate and high temperatures about 10% of the events are flares of importance 1 or larger with flares of importance 2 or larger increases significantly for high 8.6 mm brightness temperatures.

The data were also subdivided into three categories depending upon whether the daily 8.6 mm brightness temperature was increasing, constant (to within 125 K) or decreasing with time during the 24 hour interval containing the flare. No significant difference in the flare rates (for subflares and flares of class $\geq$ 1) was found (cf. Withbroe and Vernazza, 1974) when the dates were subdivided into these three categories.

The La Posta observations gave results similar to those obtained with the AFCRL data (cf. Withbroe and Vernazza, 1975). The principal difference is that for a given flare rate the 8.6 mm brightness temperature obtained from the La Posta telescope is about 150 to 200 K higher than those obtained by the AFCRL telescope. The most likely explanation for the difference is the improved spatial resolution of the La Posta telescope,

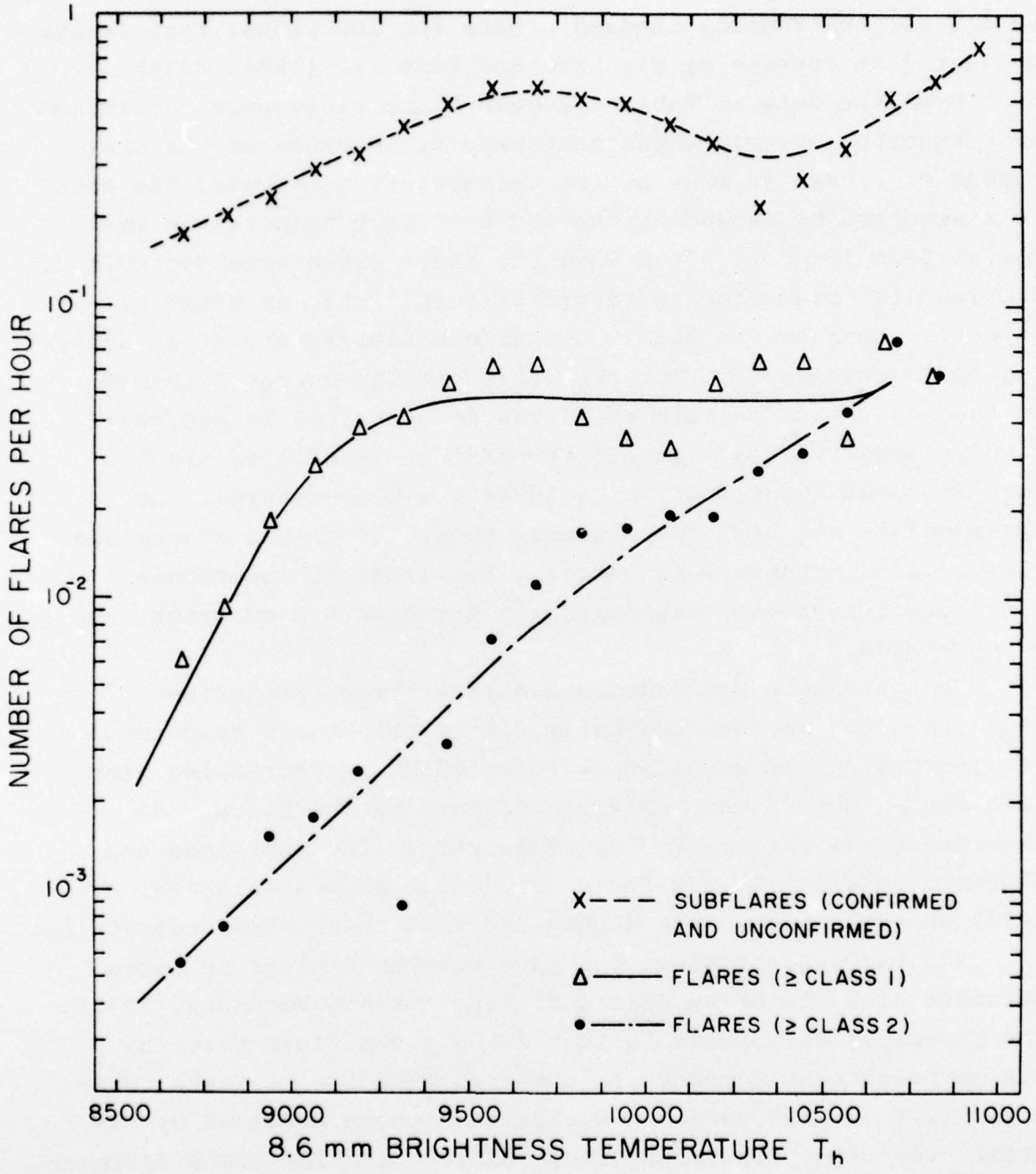

Figure 6-1. Flare rates as a function of 8.6 mm brightness temperature.

2.8 arc min, compared to 4.2 arc min for the AFCRL telescope. Because of its better spatial resolution, the La Posta telescope will tend to measure higher temperatures for active regions, since there will be less contamination by cooler surrounding quiet areas than in the AFCRL measurements made with poorer resolution.

The above results suggest that the 8.6 mm brightness temperature can be used to estimate flare probabilities. If we assume that the rate of occurrence of flares from an active region has a Poisson distribution governed by the expected number of flares per hour, then the probability of n flares occurring during the time interval Δt is given by,

$$P(n) = \frac{(N\Delta t)^n}{n!} e^{-N\Delta t} ,$$

where Δt is measured in hours and N is the number of flares per hour estimated from the measured 8.6 mm brightness temperature using the results presented in Figure 6-1. The probability of 1 or more flares occurring during that time is 1 - P (0). Thus, for example, when the 8.6 mm brightness temperature of an active region exceeds 9400 K, there is a 70% probability that one or more flares of class $\geq$ 1 will occur in that region in a 24 hour period.

Each brightness temperature used in this investigation represents an average over the area of the beam of the AFCRL radio telescope, which has a half-power beam width of 4.2 arc min. Hence hot, compact regions can have the same measured temperature as larger, cooler regions. For this reason the relationship between flare rate and 8.6 mm brightness temperature measured with a telescope having a different beam width may differ somewhat from the results given in Figure 6-1. However, the overall trends should be similar, as was demonstrated using the La Posta data (Withbroe and Vernazza, 1975).

Analyses (Vernazza and Withbroe, 1973) of EUV observations of active regions suggest that the major factor responsible for increased EUV and mm emission from the chromospheric layers of active regions (as compared to quiet regions) is the increased chromospheric electron density. This suggests that the correlation between flare rate and 8.6 mm brightness temperature implies a correlation between chromospheric electron density in active regions and the rate of flaring in these regions.

6.4 Conclusions

The results of the study suggest that observed 8.6 mm brightness temperatures of active regions can provide a quantitative means of predicting flares. One of the limitations of the currently available data is that the low spatial resolution of the measurements makes it difficult to accurately measure brightness temperatures of active regions near the limb, particularly when there are several regions close together in longitude. The low spatial resolution also makes it difficult to discriminate between brightness changes due to increased area of the active region and increased brightness per unit area. Radio observations at several wavelengths may provide a means of determining which of these factors is of greater importance in producing a correlation between flare rates and 8.6 mm brightness temperatures. The brightness temperature per unit area depends critically on the density in the area being measured. Because of the steep temperature gradients in the chromosphere (where the mm radiation is emitted) and transition layer (where the cm radiation is emitted) the ratio between the cm and mm brightness temperatures should be density sensitive and therefore may provide valuable information for flare prediction. It would be worthwhile to explore this possibility by studying relationships between flare rates and cm and mm brightness temperatures, as well as the ratio between these temperatures, measured simultaneously or nearly simultaneously in the same active regions. It would also

be worthwhile to utilize observations made more frequently than once a day in order that one can investigate possible relations between the rate of change of radio brightness temperatures and flare rates.

6.5 References

Kalaghan, P.M. and Telford, L.E.: 1970, Solar Observations at 8.6 mm Wavelength, AFCRL-70-0052, Physical Sciences Research Papers, No. 408.

Kundu, M.R.: 1959, "Sources d'Activite Solarie sur Ondes Centimetriques", Ann. Astrophys. 22, 1.

Pick-Gutmann, M.: 1961, "Evolution des Emissions Radioelectriques Solaries de Type IV et leur Relation avec d'Autres Phenomenes Solaries et Geophysiques", Ann. Astrophys. 24, 183.

Tanaka, H. and Kakinuma, T.: 1964, "The Relationship between the Spectrum of Slowly Varying Component of Solar Radio Emission and Solar Proton Event", Rep. Ionosph. Space Res. Japan 18, 32.

Vernazza, J.E., Avrett, E.H., and Loeser, R.: 1973, "Structure of the Solar Chromosphere. I. Basic Computations and Summary of Results", Astrophys. J. 184, 605.

Vernazza, J.E. and Withbroe, G.L.: 1973, "The Evolution of Solar Active Regions Based on 8.6 mm and Other Solar Observations", AFCRL-TR-73-0643, Air Force Cambridge, Research Lab., Cambridge, MA.

White, K.P., III: 1972, "Solar Flare Forecasts Based on mm-Wavelength Measurements", ATR-73 (8102)-4, Aerospace Corp., El Segundo, CA.

White, K.P., III and Mayfield, E.B.: 1973, "Final Report: Solar Flare Predictions and Warnings", ATR-73-(7298)-2, Aerospace Corp., El Segundo, CA.

White, K.P., III and Mayfield, E.B.: 1975, "Solar Flare

Predictions and Warnings: Final Report", ATR-75 (7439)-1, Aerospace Corp., El Segundo, CA.

Withbroe, G.L. and Vernazza, J.E.: 1974, "Active Region Flare Rates and 8.6 mm Brightness Temperatures", AFCRL-TR-74-0519, Air Force Cambridge Research Lab., Cambridge, MA.

Withbroe, G.L. and Vernazza, J.E.: 1975, "Active Region Flare Rates and 8.6 mm Brightness Temperatures, II", AFCRL-TR-75-0563, Air Force Cambridge Research Lab., Cambridge, MA.

Withbroe, G.L. and Vernazza, J.E.: 1976, "Active Region Flare Rates and 8.6 mm Brightness Temperatures", Solar Physics, in press.